Macro-scale models for fluid flow in tumour tissues: impact of microstructure properties

Cristina Vaghi, Raphaëlle Fanciullino, Sébastien Benzekry, Clair Poignard

Macro-scale models for fluid flow in tumour tissues: impact of microstructure properties

Cristina Vaghi[1], Raphaëlle Fanciullino[2], Sébastien Benzekry[1], Clair Poignard[1]

[1]Team MONC, Inria, Institut de Mathématiques de Bordeaux, CNRS, Bordeaux INP, Univ. Bordeaux, France

[2]SMARTc, CRCM Inserm UMR1068, CNRS UMR7258, Aix Marseille University, France

Abstract

Understanding the dynamics underlying fluid transport in tumour tissues is of fundamental importance to assess processes of drug delivery. Here, we analyse the impact of the tumour microscopic properties on the macroscopic dynamics of vascular and interstitial fluid flow. More precisely, we investigate the impact of the capillary wall permeability and the hydraulic conductivity of the interstitium on the macroscopic model arising from formal asymptotic 2-scale techniques.

The homogenization technique allows us to derive two macroscale tissue models of fluid flow that take into account the microscopic structure of the vessels and the interstitial tissue. Different regimes were derived according to the magnitude of the vessel wall permeability and the interstitial hydraulic conductivity. Importantly, we provide an analysis of the properties of the models and show the link between them. Numerical simulations were eventually performed to test the models and to investigate the impact of the microstructure on the fluid transport.

Future applications of our models include their calibration with real imaging data to investigate the impact of the tumour microenvironment on drug delivery.
Keywords: two-scale homogenisation, fluid flow in tumours, interstitial fluid pressure, tumour microscopic structure.

1 Introduction

Interstitial and capillary fluids are strongly connected in malignant tissues and are mainly involved in the transport of molecules in tumours. When drugs are intravenously injected, they have to overcome several barriers, including vascular transport, transvascular transfer, interstitial transport and finally cellular uptake [24]. The biological and physicochemical properties of the tumour microenvironment play a significant role in

the drug delivery process [9]. The geometrical microstructure of the tumour also has an important impact on the fluid flow [5].

Neoplastic tissues are highly heterogeneous. They are generally characterized by [14] accumulated solid stress [21], abnormal blood vessels network [46], elevated interstitial fluid pressure (IFP) [13], that almost equals the microvessel pressure (MVP) and dense interstitial structure [34]. These traits, that distinguish tumour tissues from normal ones, cause barriers to drug delivery [24]. The heterogeneous spatial distribution of tumour vessels and poor lymphatic drainage impair a uniform delivery of therapeutic agents in tumours. Blood vessels are unevenly distributed, leaving avascular spaces. Moreover, their walls are leaky and hyperpermeable in some places while not in other [17]. Blood flow velocity is also compromised by the elevated viscous and geometrical resistance offered by the tumour vasculature [5]. Finally, the lack of an efficient lymphatic network inside the tumour coupled with leaky tumour vessels leads to a high IFP [61] almost equal to the microvascular pressure [13]. Due to elevated IFP, the tumour interstitium is characterized by no pressure gradient [12, 25].

Several mathematical models have been developed during the last decades to investigate the features of fluid transport in the tumour microenvironment. The porous medium theory has been employed to model interstitial fluid flow (IFF) relying on Darcy's law and using average field variables defined over the whole tissue [23, 33]. Fluid transport through the blood vessels has been exploited in both discrete and continuous manners, including spatial and temporal variations. In either discrete and continuous models, the IFF and microvascular fluid (MVF) are usually coupled by Starling's law [52], that describes the fluid filtration through the highly permeable vessels walls. Microscopic models of the flow patterns around an individual capillary and a network of blood vessels have been introduced relying on the Krogh cylinder model [30, 3, 11]. Poiseuille's law can be considered to describe the blood flow in a cylindrical domain [6, 40, 50]. Furthermore, Navier-Stokes equations have been adopted to model the spatio-temporal variations in blood flow [11, 33]. More detailed biophysical models have been developed to take into account the more realistic heterogeneity of the tumour vasculature [8]. Welter et al [59] introduced an exhaustive biophysical model the incorporates tumour growth, vascular network (including arteries and veins), angiogenesis, vascular remodeling, porous medium description for the extracellular matrix (ECM) and interstitial fluid, interstitial fluid pressure and velocity and chemical entities (such as oxygen, nutrients, drugs). On the other hand, continuous models based on mixture theory have been exploited to describe interstitial and vascular fluid flow, assuming that the two phases are present at each point of the tumour [45]. Multiscale models have further been employed to investigate the coupling between tumor growth, angiogenesis, vascular remodelling and fluid transport [35] and the impact of collagen microstructure on interstitial fluid flow [60]. Imaging data have been integrated to both continuum and discrete models to quantify the effect of the heterogeneity on the fluid transport [62, 54].

The increasing amount of imaging data makes it possible to recover vascular networks

in details. However, solving discrete models on the entire vessel tree might be computationally expensive. The formal 2-scale homogenization technique allows to take into account microscopic features on the macroscopic dynamic of fluid flow. 2-scale asymptotic expansion has been previously applied to fluid and drug transport in tumours. A system of Darcy's equations has been derived in [48] to couple interstitial and vascular fluid flows in malignant tissues assuming a periodic medium. A higher complexity has been taken into account in [36], with the introduction of rheological effects in the blood flow and of local heterogeneity. A generalization of homogenized modelling for vascularized poroelastic materials has also been presented [37, 38]. More recently, higher complexity has been added to the homogenized models [49] considering three length scales for the vessel network (i.e., arteriole, venule and capillary scales).

Roughly speaking, 2 type of models have been proposed be used to describe fluid flow in tumors. Baxter and Jain suggested that simple Darcy's law can describe the experimental observations [9]. The tumor is considered as a one-phase medium at a pressure which satisfies a static diffusive equation, whose tensor reflected the global effect of the microstructure. More recently, Shipley and Chapman derived a biphasic model by 2-scale expansion techniques [48]. In their work, which was also obtained later on by Penta *et al.*, the tumour is composed of a capillary phase and an interstitium phase. Each phase is at a specific pressure and the pressures are coupled through an elliptic system which makes appear the difference between the 2 pressures. Thanks to the 2-scale expansion under periodic assumptions, the authors provide a link between the homogenised tensors and the microstructure.

The present work aims to clarify the links between the monophasic and the biphasic models. Interestingly, we enlighten about the assumptions on the microstructure that lead to the monophasic instead of the biphasic homogenised model. In particular we show that the model derived by Shipley and Chapman is the distinguished model from which the other uncouled and monphasic models might be derived under specific assumptions. In addition, our results show also that the biphasic model exhibits an exponential decay from the tumour boundary that might be difficult to capture numerically, justifying the use of monophasic model. However the appropriate boundary condition has then to be chosen, as performed in Section 3.5 .

More precisely, we compare different asymptotic regimes of the global fluid dynamics, depending on the microscopic rheological properties of the tumours. We first derive a microscopic model composed of Darcy's law for the interstitium phase and Stokes equation for the capillary phase, with a Starling's law at the interface vessel wall/interstitium. This derivation is performed thanks to an asymptotic analysis as the thickness of the capillary walls tends to zero similarly to previous works in electromagnetic studies [2, 39]. This microscopic model provides us the starting point of a formal 2-scale analysis under periodic assumption [1] to derive effective macroscale tissue models.

We provide then the asymptotic model for any order of magnitude of two parameters the permeability of the vessel wall and of the interstitial hydraulic conductivity. In

particular we show that if the interstitial hydraulic conductivity is at least as small as the wall permeability, then the model is monophasic. If the wall permeability is smaller that the interstitial hydraulic conductivity by one order of magnitude, then the two phases are coupled. In this case, the coupling is tight if the magnitude of the wall permeability is of the same order as the microstructure periodicity, and weak if it is smaller.

The characterization of the different limit models of great interest from the modelling point of view, because a cancer tissue might be composed of regions exhibiting different rheological behaviours. It is therefore important to determine how to pass from a model to another one in accordance with the microstructure properties. Eventually, numerical simulations on the macroscopic models are performed and the results are compared to the literature.

Based on the results presented in this paper, the knowledge of the tissue microstructure determines the choice of the macroscopic model, which is crucial to study the impact of the tumour microscopic characteristics on drug delivery. It is worth noting that imaging data can provide the tissue microstructure that can be integrated in the homogenised model. This modelling technique prevents the resolution of the original micro-scale model that might be unfeasible as it requires the discretisation of the entire vessel network and porous medium. Moreover, the heterogeneities of malignant tissues can be taken into account by considering the spatial variability of the micro-vessel features at the macroscopic scale.

The papers is outlined as follows. In Section 2, we present the general microscopic model that accounts for most of the phenomena encountered in living tissue. In particular thanks to an asymptotic analysis with respect to the thickness of the capillary wall, we derive a Starling's law as a transmission condition linking the interstitium and the inner capillary. This microscale model is the starting point of our formal 2-scale expansion. In Section 3, we present the formal 2-scale expansion and give the asymptotic models that are derived under different smallness assumptions on the parameters of the microscale model. We also present geometrical assumptions on the two phases –in particular in terms of connectivity– to ensure the positiveness of the resulting homogenised tensors. Numerical simulations are given in Section 4. The influence of the geometry of the microstructure on the hydraulic tensor properties is first studied. In particular, tensor anisotropy is shown when the microstructure is oriented. Then the exponential decay[1] from the tumour boundary of the difference of the interstitium and the capillary phases is evaluated in terms of the parameters and shown numerically. The conclusion section 5 puts the results in perspectives with biological applications of the results.

2 Microscopic model of fluid transport in tumours

At the microscale, the domain $\Omega \in \mathbb{R}^N$ (with $N = 2, 3$) is the medium that consists of the interstitium Ω_t, the vessel wall Ω_m and the capillary region Ω_c. The interfaces

[1]The details of the proof of this behaviour is out of the scope and given in [55].

between the inner capillary and the vessel wall on one side and between the interstitium and the vessel wall on the other side are denoted respectively by $\Gamma = \partial\Omega_c \cap \partial\Omega_m$ and $\Gamma_\delta = \partial\Omega_t \cap \partial\Omega_m$. Figure 1A shows the section of a capillary in the surrounding interstitium. In the three regions, the fluid flow is assumed to be incompressible.

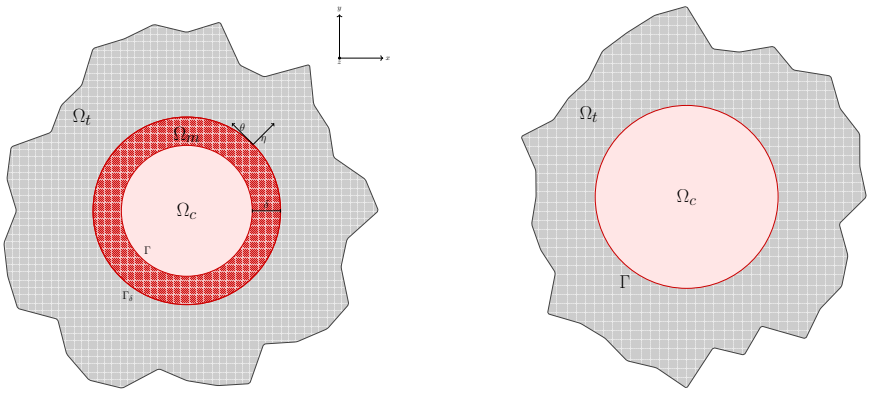

Figure 1. *Left:* schematic of the domain considered to compute the interface conditions between the capillaries and the interstitium. Ω_m denotes the vessel wall region, Γ_δ is the interface between the vessel wall and the interstitium. The transmission conditions are derived as $\delta \to 0$ using asymptotic expansion. *Right:* schematic representation of the domain of the microscopic model: section of the capillary in the sourranding tissue.

The interstitium - composed by the cells and the extracellular matrix and collagen - is modeled as an isotropic porous medium, where the velocity $\mathbf{u}_t$ and pressure p_t follow the Darcy's law:

$$\nabla \cdot \mathbf{u}_t = 0, \quad \mathbf{u}_t = -k_t \nabla p_t \qquad \text{in } \Omega_t, \tag{1a}$$

where k_t is the hydraulic conductivity in the interstitium. In the capillaries, we assume that the fluid is Newtonian with a constant viscosity μ. Neglecting the inertial effects and under the assumption of a laminar flow, the Stokes equation enables to describe the vessel velocity $\mathbf{u}_c$ and pressure p_c:

$$\nabla \cdot \mathbf{u}_c = 0, \quad \mu \nabla^2 \mathbf{u}_c = \nabla p_c \qquad \text{in } \Omega_c. \tag{1b}$$

Similarly to the interstitium, the capillary wall Ω_m - of thickness δ - is considered as a porous medium with hydraulic conductivity k_m, leading to

$$\nabla \cdot \mathbf{u}_m = 0, \quad \mathbf{u}_m = -k_m \nabla p_m \qquad \text{in } \Omega_m. \tag{1c}$$

2.1 Interface conditions

At the two boundaries Γ and Γ_δ, we have to consider interface conditions in order to couple the different equations. We make the following choices, similarly to [16]:

1. Continuity of the normal velocity on both Γ and Γ_δ:

$$\begin{aligned} \mathbf{u}_c \cdot \mathbf{n} &= \mathbf{u}_m \cdot \mathbf{n} \quad \text{on } \Gamma, \\ \mathbf{u}_t \cdot \mathbf{n} &= \mathbf{u}_m \cdot \mathbf{n} \quad \text{on } \Gamma_\delta. \end{aligned}$$

   This condition guarantees the continuity of mass through the two interfaces and it is a natural choice since the fluid is assumed to be incompressible in the three regions.

2. Balance of the normal forces at the interfaces Γ, Γ_δ:

$$p_c - \mu[(\mathbf{n} \cdot \nabla)\mathbf{u}_c] \cdot \mathbf{n} = p_m \quad \text{on } \Gamma, \tag{2}$$

$$p_t = p_m \quad \text{on } \Gamma_\delta. \tag{3}$$

   Condition (2) is due to the fact that the blood force in Ω_c acting on Γ is equal to the normal component of the Cauchy stress vector [31], while the only force in Ω_m acting on the interface is the Darcy pressure p_m. Analogously, equation (3) is motivated by the fact that the only forces acting on the interface Γ_δ are the Darcy's pressures p_m and p_t in the respective regions Ω_m and Ω_t.

3. Beavers-Joseph-Saffmann condition on the tangential component of the capillary velocity at the boundary with a porous medium Γ:

$$\mathbf{u}_c \cdot \boldsymbol{\tau} = -\frac{\sqrt{k_m \mu}}{\alpha_{\mathrm{BJ}}}[(\mathbf{n} \cdot \nabla)\mathbf{u}_c] \cdot \boldsymbol{\tau} \quad \text{on } \Gamma, \tag{4}$$

   where α_{BJ} is a constant depending on the properties of the interface. This condition comes from the experimental evidence shown by Beavers and Joseph [10] who observed that the slip velocity along Γ was proportional to the shear stress along Γ. Equation of the form (4) was derived by Saffmann using a statistical approach and the Brinkman approximation for non-homogeneous porous medium [44] .

Non-dimensionalization

In order to identify the small parameters in the above partial differential equations, it is crucial to perform a dimensional analysis. This analysis enables us to quantify the relative amplitude of the different parameters involved. We rescale our fields as follows:

$$\mathbf{x} = L\mathbf{x}', \qquad \mathbf{u} = U\mathbf{u}', \qquad p = \frac{\mu L U}{d^2} p' + p_0, \tag{5}$$

where L is the characteristic domain length, d is the mean intercapillary distance and U is a characteristic velocity. The non-dimensional fluid transport problem reads (neglecting the primes for the sake of simplicity) then as

$$\nu\nabla^2\mathbf{u}_c = \nabla p_c, \qquad \nabla\cdot\mathbf{u}_c = 0, \qquad \text{in } \Omega_c, \tag{6a}$$

$$\mathbf{u}_t = -\kappa\nabla p_c, \qquad \nabla\cdot\mathbf{u}_t = 0, \qquad \text{in } \Omega_t, \tag{6b}$$

$$\mathbf{u}_m = -\kappa_m\nabla p_m, \nabla\cdot\mathbf{u}_m = 0, \qquad \text{in } \Omega_m, \tag{6c}$$

with the interface conditions on Γ

$$\mathbf{u}_c\cdot\mathbf{n} = \mathbf{u}_m\cdot\mathbf{n} \qquad \text{on } \Gamma, \tag{6d}$$

$$p_c - \nu[(\mathbf{n}\cdot\nabla)\mathbf{u}_c]\cdot\mathbf{n} = p_m \qquad \text{on } \Gamma, \tag{6e}$$

$$\mathbf{u}_c\cdot\boldsymbol{\tau} = -R_{\boldsymbol{\tau}}[(\mathbf{n}\cdot\nabla)\mathbf{u}_c]\cdot\boldsymbol{\tau}, \text{on } \Gamma. \tag{6f}$$

and on on Γ_δ

$$\mathbf{u}_t\cdot\mathbf{n} = \mathbf{u}_m\cdot\mathbf{n} \text{on } \Gamma_\delta, \tag{6g}$$

$$p_t = p_m \qquad \text{on } \Gamma_\delta, \tag{6h}$$

where

$$\nu = \frac{d^2}{L^2}, \qquad \kappa = \frac{k_t\mu}{d^2}, \qquad \kappa_m = \frac{k_m\mu}{d^2}, \qquad R_{\boldsymbol{\tau}} = \frac{\sqrt{k_m\mu}}{\alpha_{\mathrm{BJ}}L},$$

are dimensionless quantities.

2.2 Effective Starling law to replace the thin wall of the capillary

Let us now perform the asymptotic analysis as the thickness of the capillary wall δ tends to 0, assuming that κ_m is proportional to δ with a proportionality coefficient $R_{\mathbf{n}}$ that will be defined later on:

$$\kappa_m = \delta R_{\mathbf{n}}.$$

We assume that the capillary is tubular along the direction $z \in (0, Z_0)$, where Z_0 is the characteristic length of the capillary along z. We neglect the bending along this axis. Let us denote by η the normal variable to the vessel membrane and by θ the tangential variable to the vessel wall. With these coordinates, the Laplacian is defined by

$$\nabla^2 : \frac{1}{\delta^2}\partial_\eta^2 + \frac{1}{\delta(1+\delta\zeta\eta)}\partial_\eta + \frac{1}{(1+\delta\zeta\eta)^2}\partial_\theta^2 + \partial_z^2,$$

where ζ is the curvature of the section. Identifying Ω_m and the set $\{(\eta,\theta,z) \in (0,1)\times\Gamma\times(0,Z_0)\}$, therefore, the fluid transport equations (6) in the capillary wall and the

interface conditions are rewritten as

$$\left(\partial_\eta^2 + \frac{\delta}{(1+\delta\zeta\eta)}\partial_\eta + \frac{\delta^2}{(1+\delta\zeta\eta)^2}\partial_\theta^2 + \delta^2\partial_z^2\right) p_m = 0 \qquad \text{in } \Omega_m, \quad (7a)$$

$$\mathbf{u}_c \cdot \mathbf{n} = -R_{\mathbf{n}}\partial_\eta p_m \qquad \text{on } \Gamma \quad (7b)$$

$$\partial_\eta p_m = \frac{\kappa}{R_{\mathbf{n}}}\nabla p_t \cdot \mathbf{n} \qquad \text{on } \Gamma_\delta \quad (7c)$$

$$p_c - \nu[(\mathbf{n}\cdot\nabla)\mathbf{u}_c]\cdot\mathbf{n} = p_m \qquad \text{on } \Gamma, \quad (7d)$$

$$p_t = p_m \qquad \text{on } \Gamma_\delta, \quad (7e)$$

$$\mathbf{u}_c \cdot \boldsymbol{\tau} = -R_{\boldsymbol{\tau}}[(\mathbf{n}\cdot\nabla)\mathbf{u}_c]\cdot\boldsymbol{\tau} \qquad \text{on } \Gamma \quad (7f)$$

The limit fluid flow problem at the microscale is obtained thanks to an asymptotic analysis. The formal expansion of the variables p_m, p_t, p_c and $\mathbf{u}_c$ in powers of δ

$$\begin{aligned} p_m &= p_m^{(0)} + \delta p_m^{(1)} + \delta^2 p_m^{(2)} + ... \\ p_t &= p_t^{(0)} + \delta p_t^{(1)} + \delta^2 p_t^{(2)} + ... \\ p_c &= p_c^{(0)} + \delta p_c^{(1)} + \delta^2 p_c^{(2)} + ... \\ \mathbf{u}_c &= \mathbf{u}_c^{(0)} + \delta \mathbf{u}_c^{(1)} + \delta^2 \mathbf{u}_c^{(2)} + ... \end{aligned}$$

is injected in the equations. Equating coefficients of order $1(=\delta^0)$ in (7a)-(7f), we obtain the following system of equations

$$\partial_\eta^2 p_m^{(0)} = 0 \qquad \text{in } \Omega_m \quad (8a)$$

$$\mathbf{u}_c^{(0)} \cdot \mathbf{n} = -R_{\mathbf{n}}\partial_\eta p_m^{(0)} \qquad \text{on } \Gamma \quad (8b)$$

$$\partial_\eta p_m^{(0)} = \frac{\kappa}{R_{\mathbf{n}}}\nabla p_t^{(0)} \cdot \mathbf{n} \qquad \text{on } \Gamma_\delta \quad (8c)$$

$$p_c^{(0)} - \nu[(\mathbf{n}\cdot\nabla)\mathbf{u}_c^{(0)}]\cdot\mathbf{n} = p_m^{(0)} \qquad \text{on } \Gamma \quad (8d)$$

$$p_m^{(0)} = p_t^{(0)} \qquad \text{on } \Gamma_\delta \quad (8e)$$

$$\mathbf{u}_c^{(0)} \cdot \boldsymbol{\tau} = -R_{\boldsymbol{\tau}}[(\mathbf{n}\cdot\nabla)\mathbf{u}_c^{(0)}]\cdot\boldsymbol{\tau} \qquad \text{on } \Gamma \quad (8f)$$

From (8a) and (8c) we infer

$$\partial_\eta p_m^{(0)} = \frac{\kappa}{R_{\mathbf{n}}}\nabla p_t^{(0)} \cdot \mathbf{n} \qquad \text{in } \Omega_m. \quad (9)$$

Equations (9) and (8d) then lead to

$$p_m^{(0)} = \left(\frac{\kappa}{R_{\mathbf{n}}}\nabla p_t^{(0)} \cdot \mathbf{n}\right)\eta + p_c^{(0)} - \nu[(\mathbf{n}\cdot\nabla)\mathbf{u}_c^{(0)}]\cdot\mathbf{n} \qquad \text{in } \Omega_m. \quad (10)$$

from which we infer thanks to (8e) the expression of $p_t^{(0)}$:

$$p_t^{(0)} = p_m^{(0)}(\eta = 1) = \frac{\kappa}{R_{\mathbf{n}}} \nabla p_t^{(0)} \cdot \mathbf{n} + p_c^{(0)} - \nu[(\mathbf{n} \cdot \nabla)\mathbf{u}_c^{(0)}] \cdot \mathbf{n} \qquad \text{on } \Gamma_\delta. \tag{11}$$

From equations (11), (8b) and (8c) we derive formally the boundary conditions for small δ:

$$\kappa \nabla p_t^{(0)} \cdot \mathbf{n} = R_{\mathbf{n}} \left(p_t^{(0)} - p_c^{(0)} + \nu[(\mathbf{n} \cdot \nabla)\mathbf{u}_c^{(0)}] \cdot \mathbf{n} \right) \qquad \text{on } \Gamma, \tag{12a}$$

$$\mathbf{u}_c^{(0)} \cdot \mathbf{n} = -\kappa \nabla p_t^{(0)} \cdot \mathbf{n} \qquad \text{on } \Gamma, \tag{12b}$$

$$\mathbf{u}_c^{(0)} \cdot \boldsymbol{\tau} = -R_{\boldsymbol{\tau}}[(\mathbf{n} \cdot \nabla)\mathbf{u}_c^{(0)}] \cdot \boldsymbol{\tau} \qquad \text{on } \Gamma. \tag{12c}$$

Transmission conditions (12a)-(12b) can be rewritten as

$$\mathbf{u}_t \cdot \mathbf{n} = \mathbf{u}_c \cdot \mathbf{n} = R_{\mathbf{n}}(p_c - p_t - \nu[(\mathbf{n} \cdot \nabla)\mathbf{u}_c] \cdot \mathbf{n}) \qquad \text{on } \Gamma, \tag{13}$$

which is similar to Starling's law, that is the most widely used equation in literature to model flux transport across the vessel wall [25, 6] and reads

$$\mathbf{u}_c \cdot \mathbf{n} = L_p(p_c - p_t - \sigma\,(\pi_c - \pi_t)),$$

where L_p is the vascular permeability, σ is the osmotic reflection coefficient ($\sigma \in (0, 1)$) that expresses the glycocalyx filter function through the endothelial wall and $(\pi_c - \pi_t)$ is the oncotic pressure difference between the capillaries and the interstitium. However, the latter can be considered negligible compared to the interstitial fluid pressure difference in tumors [23, 57]. Moreover, the viscous term in equation (13) is usually neglected but it is necessary to guarantee the well-posedness of the problem and does not change the physical meaning since it is based on the balance of the normal forces [36].

The parameters $R_{\mathbf{n}}$ and L_p are linked by $R_{\mathbf{n}} = \dfrac{L_p L \mu}{d^2}$. Therefore, the limit microscopic model reads as

$$\nu \nabla^2 \mathbf{u}_c = \nabla p_c, \qquad \nabla \cdot \mathbf{u}_c = 0, \qquad \text{in } \Omega_c, \tag{14a}$$

$$\mathbf{u}_t = -\kappa \nabla p_c, \qquad \nabla \cdot \mathbf{u}_t = 0, \qquad \text{in } \Omega_t, \tag{14b}$$

$$\mathbf{u}_c \cdot \mathbf{n} = \mathbf{u}_t \cdot \mathbf{n} \qquad \text{on } \Gamma, \tag{14c}$$

$$\mathbf{u}_c \cdot \mathbf{n} = R_{\mathbf{n}} \left(p_c - p_t - \nu[(\mathbf{n} \cdot \nabla)\mathbf{u}_c] \cdot \mathbf{n} \right) \qquad \text{on } \Gamma, \tag{14d}$$

$$\mathbf{u}_c \cdot \boldsymbol{\tau} = -R_{\boldsymbol{\tau}}[(\mathbf{n} \cdot \nabla)\mathbf{u}_c] \cdot \boldsymbol{\tau}, \qquad \text{on } \Gamma, \tag{14e}$$

where

$$\nu = \frac{d^2}{L^2}, \qquad \kappa = \frac{k_t \mu}{d^2}, \qquad R_{\mathbf{n}} = \frac{L_p L \mu}{d^2}, \qquad R_{\boldsymbol{\tau}} = \frac{\sqrt{k_m \mu}}{\alpha_{\mathrm{BJ}} L},$$

are dimensionless quantities depending on the microscopic properties of the tissue.

3 Formal derivation of continuum macroscale models for different regimes

This section is devoted to the derivation of a continuum macro-scale models from the microscopic model (14) using the 2-scale asymptotic expansion method [4, 15, 1] and under different asymptotic regimes depending on the capillary wall permeability and the hydraulic conductivity of the interstitium.

3.1 Geometrical setting

Let us first present the geometrical setting. We assume that d is the mean inter-capillary distance and L is the tissue characteristic length such that $\varepsilon = d/L \ll 1$. We denote by Y the reference periodic unit cell that $[0,1]^N$. It is composed by the interstitium Y_t and the capillaries Y_c. The interface between Y_t and Y_c is denoted Γ_Y. The normal vector $\mathbf{n}$ to the interface Γ_Y is directed outwardlry from the vascular domain Y_c towards Y_t. The total domain Ω is divided periodically in each direction in squares Y_n^ε such that

$$Y_n^\varepsilon = \varepsilon n + \varepsilon Y, \qquad Y_{t,n}^\varepsilon = \varepsilon n + \varepsilon Y_t, \quad Y_{c,n}^\varepsilon = \varepsilon n + \varepsilon Y_c, \quad \Gamma_n^\varepsilon = \varepsilon n + \varepsilon \Gamma_Y, \quad \forall n \in \mathbb{Z}^N.$$

The difficult problem of the boundary conditions and their influence on the expansion is out of the scope of the paper. The reader may consider Ω as a manifold without boundary, for instance the unit cube with periodic condition.

The domain Ω is thus composed of two subdomains $\Omega_t^\varepsilon = \cup_n Y_{t,n}^\varepsilon$ and $\Omega_c^\varepsilon = \cup_n Y_{c,n}^\varepsilon$ that depend on ε and are connected when $N = 3$. The interface between the two subdomains is $\Gamma^\varepsilon = \cup_n \Gamma_n^\varepsilon$. Figure 2 shows a schematic illustration of the periodic domain and of the unitary cell Y.

3.2 The fluid flow model and the 3 asymptotic regimes

The fluid flow model reads in the oscillating domain $\Omega = \Omega_c^\varepsilon \cup \Omega_t^\varepsilon \cup \Gamma^\varepsilon$ as:

$$\nu \nabla^2 \mathbf{u}_c^\varepsilon = \nabla p_c^\varepsilon + \mathbf{f}_c, \qquad \nabla \cdot \mathbf{u}_c^\varepsilon = 0, \qquad \text{in } \Omega_c^\varepsilon, \tag{15a}$$

$$\mathbf{u}_t^\varepsilon = -\kappa \nabla p_t^\varepsilon, \qquad \nabla \cdot \mathbf{u}_t^\varepsilon = 0, \qquad \text{in } \Omega_t^\varepsilon, \tag{15b}$$

$$\mathbf{u}_c^\varepsilon \cdot \mathbf{n} = \mathbf{u}_t^\varepsilon \cdot \mathbf{n} \qquad \text{on } \Gamma^\varepsilon, \tag{15c}$$

$$\mathbf{u}_c^\varepsilon \cdot \mathbf{n} = R_{\mathbf{n}} \left(p_c^\varepsilon - p_t^\varepsilon - \nu [(\mathbf{n} \cdot \nabla)\mathbf{u}_c^\varepsilon] \cdot \mathbf{n} \right) \qquad \text{on } \Gamma^\varepsilon, \tag{15d}$$

$$\mathbf{u}_c^\varepsilon \cdot \boldsymbol{\tau} = -R_{\boldsymbol{\tau}} [(\mathbf{n} \cdot \nabla)\mathbf{u}_c^\varepsilon] \cdot \boldsymbol{\tau}, \qquad \text{on } \Gamma^\varepsilon. \tag{15e}$$

As mention previously, no boundary conditions are considered in this section to avoid the emergence of boundary layers that prevent the following derivation. Since these boundary layers are exponentially decaying, their influence is restricted to the vicinityof the boundary. The source term f_c is supposed infinitely smooth ni Ω_c^ε. While it is natural

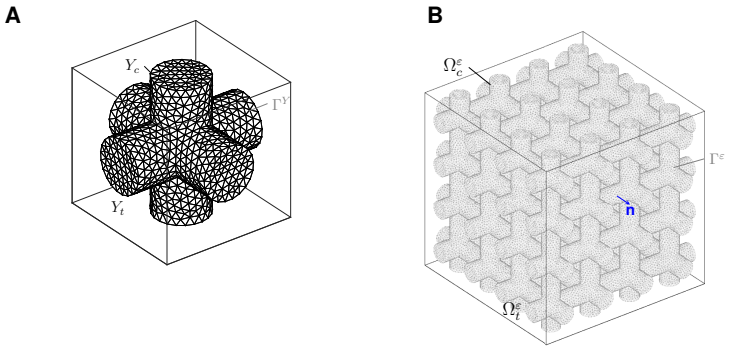

Figure 2. Unitary cell $Y = [0,1]^3$ (left) composed by the capillary region Y_c and the interstitial compartment Y_t; the interface between the two regions is denoted by Γ_Y. Periodic domain Ω (right): the tumour capillaries Ω_c^ε are assumed to be in the tubes, while the outer region corresponds to the interstitial compartment Ω_t^ε; the interface between the two regions is denoted by Γ^ε and the normal $\mathbf{n}$ is directed outward the vascular domain.

to consider the scaling $\nu = O(\varepsilon^2)$ on the viscosity to avoid trivial limit, the parameters $R_{\mathbf{n}}$, and κ are then taken as

$$\nu = \varepsilon^2 \bar{\nu}, \qquad R_{\mathbf{n}} = \varepsilon^\gamma \bar{R}_{\mathbf{n}}, \qquad \kappa = \varepsilon^\eta \bar{\kappa} \tag{16}$$

so that $\bar{\nu}$, $\bar{R}_{\mathbf{n}}$ and $\bar{\kappa}$ are of order 1. Shipley *et al.* and Penta *et al.* have considered previsouls the cas $\gamma = 1, \eta = 0$ [48], while we consider here the cases $(\gamma, \eta) \in \mathbb{N}^2$.

3.3 Heuristics of the formal 2-scale expansion

According to the multiple scales theory, it is natural to introduce the fast variable $\mathbf{y} = \mathbf{x}/\varepsilon$. The idea of the 2-scale expansion consists in assuming that any field g^ε appearing in the problem (15) – g^ε stands for $\mathbf{u}_c^\varepsilon$, $\mathbf{u}_t^\varepsilon$, p_c^ε and p_t^ε – has an expansion under the form

$$g^\varepsilon(\mathbf{x}) = \sum_{\ell=0}^{\infty} \varepsilon^\ell g^{(\ell)}(\mathbf{x}, \mathbf{x}/\varepsilon), \qquad \forall \mathbf{x} \in \Omega,$$

where the fields $(\mathbf{x}, \mathbf{y}) \mapsto g^{(\ell)}(\mathbf{x}, \mathbf{y})$ are Y-periodic at any order $\ell \geq 0$. In order to identify the problem satisfied by each field $g^{(\ell)}$, it is crucial to rewrite the differential operators as

$$\nabla = \nabla_{\mathbf{x}} + \frac{1}{\varepsilon}\nabla_{\mathbf{y}}, \qquad \nabla \cdot = \nabla_{\mathbf{x}} \cdot + \frac{1}{\varepsilon}\nabla_{\mathbf{y}} \cdot, \qquad \nabla^2 = \nabla_{\mathbf{x}}^2 + \frac{2}{\varepsilon}\nabla_{\mathbf{x}} \cdot \nabla_{\mathbf{y}} + \frac{1}{\varepsilon^2}\nabla_{\mathbf{y}}^2 \cdot.$$

Problem (15) is then rewritten in the variables $(\mathbf{x}, \mathbf{y})$, making appear the asymptotic

parameter ε and the parameters (γ, η):

$$\bar{\nu}\left(\nabla_{\mathbf{y}}^2 \mathbf{u}_c^\varepsilon + 2\varepsilon \nabla_{\mathbf{y}} \cdot \nabla_{\mathbf{x}} \mathbf{u}_c^\varepsilon + \varepsilon^2 \nabla_{\mathbf{x}}^2 \mathbf{u}_c^\varepsilon\right) = \frac{1}{\varepsilon} \nabla_{\mathbf{y}} p_c^\varepsilon + \nabla_{\mathbf{x}} p_c^\varepsilon + \mathbf{f}_c \qquad \text{in } \Omega_c^\varepsilon \times Y_c, \tag{17a}$$

$$\frac{1}{\varepsilon} \nabla_{\mathbf{y}} \cdot \mathbf{u}_c^\varepsilon + \nabla_{\mathbf{x}} \cdot \mathbf{u}_c^\varepsilon = 0 \qquad \text{in } \Omega_c^\varepsilon \times Y_c, \tag{17b}$$

$$\frac{1}{\varepsilon^2} \nabla_{\mathbf{y}}^2 p_t^\varepsilon + \frac{2}{\varepsilon} \nabla_{\mathbf{x}} \cdot \nabla_{\mathbf{y}} p_t^\varepsilon + \nabla_{\mathbf{x}}^2 p_t^\varepsilon = 0 \qquad \text{in } \Omega_t^\varepsilon \times Y_t. \tag{17c}$$

The interface conditions on $\Gamma^\varepsilon \times \Gamma_Y$,vary according to the value of γ and η :

$$\frac{1}{\varepsilon^\gamma \bar{R}_{\mathbf{n}}} \mathbf{u}_c^\varepsilon \cdot \mathbf{n} + (p_t^\varepsilon - p_c^\varepsilon) + \varepsilon \bar{\nu} [(\mathbf{n} \cdot \nabla_{\mathbf{y}}) \mathbf{u}_c^\varepsilon] \cdot \mathbf{n} + \varepsilon^2 \bar{\nu} [(\mathbf{n} \cdot \nabla_{\mathbf{x}}) \mathbf{u}_c^\varepsilon] \cdot \mathbf{n} = 0, \tag{17d}$$

$$\frac{1}{\varepsilon} [(\mathbf{n} \cdot \nabla_{\mathbf{y}}) \mathbf{u}_c^\varepsilon] \cdot \boldsymbol{\tau} + [(\mathbf{n} \cdot \nabla_{\mathbf{x}}) \mathbf{u}_c^\varepsilon] \cdot \boldsymbol{\tau} + \frac{1}{R_{\boldsymbol{\tau}}} \mathbf{u}_c^\varepsilon \cdot \boldsymbol{\tau} = 0, \tag{17e}$$

$$\varepsilon^\eta \bar{\kappa} \nabla_{\mathbf{y}} p_t^\varepsilon \cdot \mathbf{n} + \varepsilon \mathbf{u}_c^\varepsilon \cdot \mathbf{n} + \varepsilon^{1+\eta} \bar{\kappa} \nabla_{\mathbf{x}} p_t^\varepsilon \cdot \mathbf{n} = 0. \tag{17f}$$

3.3.1 Formal cascade of equalities

Injecting the expansions in power of ε, we infer the following cascade of equations linking formally the coefficients $(\mathbf{u}_c^k, \mathbf{u}_t^k, p_c^k, p_t^k)$, with the usual convention that $(\mathbf{u}_c^\ell, \mathbf{u}_t^\ell, p_c^\ell, p_t^\ell) = (0,0,0,0)$ for any index ℓ strictly negative:

$$-\nabla_{\mathbf{y}} p_c^k + \bar{\nu} \nabla_{\mathbf{y}}^2 \mathbf{u}_c^{k-1} - \nabla_{\mathbf{x}} p_c^{k-1} + 2\nabla_{\mathbf{y}} \cdot \nabla_{\mathbf{x}} \mathbf{u}_c^{k-2} + \nabla_{\mathbf{x}}^2 \mathbf{u}_c^{k-3} = \delta_1^k \mathbf{f}_c, \text{ in } \Omega_c^\varepsilon \times Y_c, \tag{18a}$$

$$\nabla_{\mathbf{y}} \cdot \mathbf{u}_c^{k-1} + \nabla_{\mathbf{x}} \cdot \mathbf{u}_c^{k-2} = 0 \qquad \text{in } \Omega_c^\varepsilon \times Y_c, \tag{18b}$$

$$\nabla_{\mathbf{y}}^2 p_t^k + 2\nabla_{\mathbf{x}} \cdot \nabla_{\mathbf{y}} p_t^{k-1} + \nabla_{\mathbf{x}}^2 p_t^{k-2} = 0 \qquad \text{in } \Omega_t^\varepsilon \times Y_t. \tag{18c}$$

The interface conditions on $\Gamma^\varepsilon \times \Gamma_Y$,vary according to the value of γ and η :

$$\begin{aligned} \frac{1}{\bar{R}_{\mathbf{n}}} \mathbf{u}_c^{k-1} \cdot \mathbf{n} + (p_t^{k-1-\gamma} - p_c^{k-1-\gamma}) + \bar{\nu} [(\mathbf{n} \cdot \nabla_{\mathbf{y}}) \mathbf{u}_c^{k-2-\gamma}] \cdot \mathbf{n} \\ + \bar{\nu} [(\mathbf{n} \cdot \nabla_{\mathbf{x}}) \mathbf{u}_c^{k-3-\gamma}] \cdot \mathbf{n} = 0, \end{aligned} \tag{18d}$$

$$[(\mathbf{n} \cdot \nabla_{\mathbf{y}}) \mathbf{u}_c^{k-1}] \cdot \boldsymbol{\tau} + [(\mathbf{n} \cdot \nabla_{\mathbf{x}}) \mathbf{u}_c^{k-2}] \cdot \boldsymbol{\tau} + \frac{1}{R_{\boldsymbol{\tau}}} \mathbf{u}_c^{k-2} \cdot \boldsymbol{\tau} = 0, \tag{18e}$$

$$\mathbf{u}_c^{k+\eta-1} \cdot \mathbf{n} + \bar{\kappa} \nabla_{\mathbf{y}} p_t^k \cdot \mathbf{n} + \bar{\kappa} \nabla_{\mathbf{x}} p_t^{k-1} \cdot \mathbf{n} = 0. \tag{18f}$$

3.3.2 Derivation of the leading term

The above equalities (26) enables us to derive successively –and formally– the coefficients $(\mathbf{u}_c^k, \mathbf{u}_t^k, p_c^k, p_t^k)$. Our main interest here is to derive the leading term for different value of $(\gamma, \eta) \in \mathbb{N}^2$.

• First, taking $k = 0$ in (18a), we infer that $\nabla_{\mathbf{y}} p_c^0 = 0$, hence p_c^0 depends only on $\mathbf{x}$:

$$p_c^0 = p_c^0(\mathbf{x}).$$

Then consider the problem satisfied by p_t^0. If $\gamma - \eta \geq 0$, it reads:

$$\begin{aligned}
&\nabla_{\mathbf{y}}^2 p_t^0 = 0, \quad \text{in } Y_t \\
&\bar{\kappa} \nabla_{\mathbf{y}} p_t^0 \cdot \mathbf{n} = -\mathbf{u}_c^{\eta-1} \cdot \mathbf{n} = \bar{R}_{\mathbf{n}} (p_t^{\eta-1-\gamma} - p_c^{\eta-1-\gamma}), \quad \text{on } \Gamma_Y
\end{aligned}$$

hence $\nabla_{\mathbf{y}} p_t^0 \cdot \mathbf{n} = 0$ since $\eta - 1 - \gamma \leq -1$, and thus similarly to p_c^0, the pressure p_t^0 depends only on $\mathbf{x}$. If $\gamma - \eta \leq -1$, the problem satisfied by p_t^0 reads:

$$\begin{aligned}
&\nabla_{\mathbf{y}}^2 p_t^0 = 0, \quad \text{in } Y_t \\
&\bar{R}_{\mathbf{n}} (p_t^0 - p_c^0) = -\mathbf{u}_c^{\gamma} \cdot \mathbf{n} = -\bar{\kappa} \nabla_{\mathbf{y}} p_t^{1+\gamma-\eta} \cdot \mathbf{n}, \quad \text{on } \Gamma_Y.
\end{aligned}$$

We then infer that if $\gamma - \eta \leq -1$, the only solution of the above equation is

$$p_t^0 = p_t^0(\mathbf{x}) = p_c^0(x).$$

We thus have shown that whatever the couple $(\gamma, \eta) \in \mathbb{N}^2$, p_c^0 and p_t^0 depends only on $\mathbf{x}$, and even $p_t^0(\mathbf{x}) = p_c^0(x)$ if $\gamma - \eta - 1 \leq 0$.

• Then, taking $k = 1$, we infer that $(\mathbf{u}_c^0, p_c^1)$ satisfies the following problem set in Y_c:

$$-\nabla_{\mathbf{y}} p_c^1 + \bar{\nu} \nabla_{\mathbf{y}}^2 \mathbf{u}_c^0 = \nabla_{\mathbf{x}} p_c^0 + \mathbf{f}_c, \tag{19a}$$

$$\nabla_{\mathbf{y}} \cdot \mathbf{u}_c^0 = 0 \tag{19b}$$

$$\frac{1}{\bar{R}_{\mathbf{n}}} \mathbf{u}_c^0 \cdot \mathbf{n} = -(p_t^{-\gamma} - p_c^{-\gamma}), \tag{19c}$$

$$[(\mathbf{n} \cdot \nabla_{\mathbf{y}}) \mathbf{u}_c^0] \cdot \boldsymbol{\tau} = 0. \tag{19d}$$

Using the compatibility condition on the divergence, we infer that whatever $\gamma \in \mathbb{N}$:

$$\bar{R}_{\mathbf{n}} \int_{\Gamma_Y} (p_t^{-\gamma} - p_c^{-\gamma}) dy = \int_{Y_c} \nabla_{\mathbf{y}} \cdot \mathbf{u}_c^0 \, dy = 0.$$

Note that this result is compatible with the convention if $\gamma \geq 1$, and it says that if $\gamma = 0$, then

$$p_t^0(\mathbf{x}) = p_c^0(\mathbf{x}).$$

Thanks to the following corrector $(\mathbf{W}^j, \mathrm{P}^j)_{j=1,\cdots,N}$ where N is the dimension (equal to

2 or 3 here):

$$\bar{\nu}\nabla^2_{\mathbf{y}}\mathbf{W}^j + \mathbf{e}_j = \nabla_{\mathbf{y}}\mathrm{P}^j \qquad \text{in } Y_c, \tag{20a}$$

$$\nabla_{\mathbf{y}} \cdot \mathbf{W}^j = 0 \qquad \text{in } Y_c, \tag{20b}$$

$$\mathbf{W}^j \cdot \mathbf{n} = 0 \qquad \text{on } \Gamma_Y, \tag{20c}$$

$$[(\mathbf{n} \cdot \nabla_{\mathbf{y}})\mathbf{W}^j] \cdot \boldsymbol{\tau} = 0 \qquad \text{on } \Gamma_Y, \tag{20d}$$

the coefficients $(\mathbf{u}_c^0, p_c^1)$ reads as

$$\mathbf{u}_c^{(0)}(\mathbf{x},\mathbf{y}) = -\sum_{j=1j}^{N} \mathbf{W}^j \left(\left(\nabla_{\mathbf{x}} p_c^{(0)} + \mathbf{f}_c \right) \cdot \mathbf{e}_j \right) := -\underline{\mathcal{W}}(\mathbf{y}) \left(\nabla_{\mathbf{x}} p_c^0(\mathbf{x}) + \mathbf{f}_c \right), \tag{21}$$

$$\begin{aligned} p_c^{(1)}(\mathbf{x},\mathbf{y}) &= -\sum_{j=1}^{N} P^j \left(\left(\nabla_{\mathbf{x}} p_c^{(0)} + \mathbf{f}_c \right) \cdot \mathbf{e}_j \right) + \bar{p}_c^{(1)}(\mathbf{x}) \\ &:= -\mathcal{P}(\mathbf{y}) \cdot \left(\nabla_{\mathbf{x}} p_c^0(\mathbf{x}) + \mathbf{f}_c \right) + \bar{p}_c^{(1)}(\mathbf{x}), \end{aligned} \tag{22}$$

Consider now p_t^1. It satisfies

$$\nabla^2_{\mathbf{y}} p_t^1 = 0, \quad \text{in } Y_t \tag{23a}$$

$$\bar{\kappa}\nabla_{\mathbf{y}} p_t^1 \cdot \mathbf{n} = -\bar{\kappa}\nabla_{\mathbf{x}} p_t^0 \cdot \mathbf{n} - \mathbf{u}_c^{\eta} \cdot \mathbf{n}, \quad \text{on } \Gamma_Y \tag{23b}$$

If $\gamma - \eta \geq 0$, we have

$$\bar{\kappa}\nabla_{\mathbf{y}} p_t^1 \cdot \mathbf{n} = -\bar{\kappa}\nabla_{\mathbf{x}} p_t^0 \cdot \mathbf{n} + \bar{R}_{\mathbf{n}}(p_t^{\eta-\gamma} - p_c^{\eta-\gamma}) = -\bar{\kappa}\nabla_{\mathbf{x}} p_t^0 \cdot \mathbf{n} + \delta_0^{\eta-\gamma}\bar{R}_{\mathbf{n}}(p_t^0 - p_c^0), \quad \text{on } \Gamma_Y.$$

Using the compatibility condition we infer that if $\eta = \gamma$ then necessarily $p_t^0 = p_c^0$. Moreover defining G^j, such that :

$$\nabla^2_{\mathbf{y}}\mathrm{G}^j = 0 \qquad \text{in } Y_t \tag{24a}$$

$$\nabla_{\mathbf{y}}\mathrm{G}^j \cdot \mathbf{n} = \mathbf{n} \cdot \mathbf{e}_j \qquad \text{on } \Gamma_Y, \tag{24b}$$

then if $\gamma - \eta \geq 0$ we infer that p_t^1 reads as

$$p_t^1(\mathbf{x},\mathbf{y}) = -\sum_{j=1}^{N} G^j \left(\nabla_{\mathbf{x}} p_t^{(0)} \cdot \mathbf{e}_j \right) + \bar{p}_t^1(\mathbf{x}) := -\mathcal{G}(\mathbf{y}) \cdot \nabla_{\mathbf{x}} p_t^0(\mathbf{x}) + \bar{p}_t^1(\mathbf{x}). \tag{25}$$

• Now, taking $k=2$, we infer that $(\mathbf{u}_c^1, p_c^2)$ satisfies the following problem set in Y_c:

$$-\nabla_{\mathbf{y}} p_c^2 + \bar{\nu}\nabla_{\mathbf{y}}^2 \mathbf{u}_c^1 = \nabla_{\mathbf{x}} p_c^1 - 2\bar{\nu}\nabla_{\mathbf{y}} \cdot \nabla_{\mathbf{x}} \mathbf{u}_c^0, \tag{26a}$$

$$\nabla_{\mathbf{y}} \cdot \mathbf{u}_c^1 = -\nabla_{\mathbf{x}} \cdot \mathbf{u}_c^0 \tag{26b}$$

$$\frac{1}{\bar{R}_{\mathbf{n}}} \mathbf{u}_c^1 \cdot \mathbf{n} = -(p_t^{1-\gamma} - p_c^{1-\gamma}) - [(\mathbf{n} \cdot \nabla_{\mathbf{y}}) \mathbf{u}_c^{-\gamma}] \cdot \mathbf{n}, \tag{26c}$$

$$[(\mathbf{n} \cdot \nabla_{\mathbf{y}}) \mathbf{u}_c^2] \cdot \boldsymbol{\tau} = -[(\mathbf{n} \cdot \nabla_{\mathbf{y}}) \mathbf{u}_c^0] \cdot \boldsymbol{\tau} - \frac{1}{R_{\boldsymbol{\tau}}} \mathbf{u}_c^0 \cdot \boldsymbol{\tau}. \tag{26d}$$

Using the compatibility condition on the divergence, we infer that for any $\gamma \geq 1$:

$$\nabla \cdot \left(\frac{1}{Y_c} \int_{Y_c} \underline{\mathcal{W}}(\mathbf{y}) \left(\nabla_{\mathbf{x}} p_c^0 + \mathbf{f}_c \right) \right) + \delta_1^\gamma \bar{R}_{\mathbf{n}} \frac{|\Gamma|}{|Y_c|} (p_t^0 - p_c^0) = 0,$$

where δ_1^γ is the Kronecker symbol equal to 1 if $\gamma = 1$ and 0 elsewhere.

If $\gamma - \eta \geq 1$, the coefficient p_2^t satisfies:

$$\nabla_{\mathbf{y}}^2 p_t^2 = -2\nabla_{\mathbf{y}} \cdot \nabla_{\mathbf{y}} p_t^1 - \nabla_{\mathbf{x}}^2 p_t^0, \quad \text{in } Y_t$$
$$\bar{\kappa}\nabla_{\mathbf{y}} p_t^2 \cdot \mathbf{n} = -\bar{\kappa}\nabla_{\mathbf{x}} p_t^1 \cdot \mathbf{n} - \mathbf{u}_c^{1+\eta} \cdot \mathbf{n} = -\bar{\kappa}\nabla_{\mathbf{x}} p_t^1 \cdot \mathbf{n} + \bar{R}_{\mathbf{n}} (p_t^{1+\eta-\gamma} - p_c^{1+\eta-\gamma}).$$

Integrating over Y_t, one infers the problem satisfied by p_t^0 if $\gamma - \eta \geq 1$:

$$\nabla \cdot \left(\kappa \left(\mathbb{I} - \frac{1}{Y_t} \int_{Y_t} \mathcal{G}(\mathbf{y}) \right) \nabla_{\mathbf{x}} p_t^0 \right) - \delta_1^{\gamma-\eta} \bar{R}_{\mathbf{n}} \frac{|\Gamma|}{|Y_t|} (p_t^0 - p_c^0) = 0,$$

It remains to consider the case $\gamma = 0$. Suppose first $\gamma = 0, \eta = 0$. The pressure p_t^2 satisfies

$$\nabla_{\mathbf{y}}^2 p_t^2 = -2\nabla_{\mathbf{y}} \cdot \nabla_{\mathbf{y}} p_t^1 - \nabla_{\mathbf{x}}^2 p_t^0, \quad \text{in } Y_t$$
$$\bar{\kappa}\nabla_{\mathbf{y}} p_t^2 \cdot \mathbf{n} = -\bar{\kappa}\nabla_{\mathbf{x}} p_t^1 \cdot \mathbf{n} - \mathbf{u}_c^1 \cdot \mathbf{n}.$$

We already know that

$$p_t^1 = -\mathcal{G} \cdot \nabla_{\mathbf{x}} p_t^0(x), \quad \mathbf{u}_c^0 = \underline{\mathcal{W}} \left(\nabla_{\mathbf{x}} p_c^0 + \mathbf{f}_c \right)$$

and

$$\int_{\Gamma_Y} \mathbf{u}_c^1 \cdot \mathbf{n} dy = \int_{Y_c} \nabla_{\mathbf{y}} \cdot \mathbf{u}_c^1 dy = -\nabla_{\mathbf{x}} \cdot \int_{Y_c} \mathbf{u}_c^0 dy,$$

Then integrating over Y_t implies that

$$\nabla_{\mathbf{x}} \cdot \left(\kappa \left(\mathbb{I} - \frac{1}{Y_t} \int_{Y_t} \mathcal{G} dy \right) \nabla_{\mathbf{x}} p_t^0 \right) = -\nabla_{\mathbf{x}} \cdot \left(\frac{1}{|Y_t|} \int_{Y_c} \underline{\mathcal{W}} dy \left(\nabla_{\mathbf{x}} p_c^0 + \mathbf{f}_c \right) \right).$$

Consider now $\gamma = 0, \eta = 1$. Using (23), we infer the compatibility condition:

$$0 = \int_{\Gamma_Y} \mathbf{u}_c^1 \cdot n dy = -\nabla_{\mathbf{x}} \cdot \int_{Y_c} \mathbf{u}_c^0 dy.$$

If $\eta \geq 2$, we have successively

$$-\nabla_{\mathbf{x}} \cdot \int_{Y_c} \mathbf{u}_c^0 dy = \int_{Y_c} \nabla_{\mathbf{y}} \cdot \mathbf{u}_c^1 dy = \int_{\Gamma_Y} \mathbf{u}_c^1 \cdot n dy = -\int_{\Gamma_Y} \bar{\kappa} \nabla_{\mathbf{y}} p_t^{2-\eta} - \int_{\Gamma_Y} \bar{\kappa} \nabla_{\mathbf{x}} p_t^{1-\eta} = 0.$$

Hence for any $\eta \geq 1$ and $\gamma = 0$, $p_c^0 = p_t^0$ satisfies

$$\nabla \cdot \left(\frac{1}{|Y_c|} \int_{Y_c} \underline{\mathcal{W}}(\mathbf{y}) \left(\nabla_{\mathbf{x}} p_c^0 + \mathbf{f}_c \right) \right) = 0.$$

To summarize, the following proposition has been shown.

Proposition 3.1. *Denoting by $z \mapsto \chi_H(z)$ the Heaviside function equal to 1 if $z \geq 0$ and 0 elsewhere, we have shown formally that the leading order terms p_c^0, p_t^0 of the expansion satisfies, for any $(\gamma, \eta) \in \mathbb{N}^2$:*

$$\nabla \cdot \left(\boldsymbol{E} \nabla_{\boldsymbol{x}} p_c^0 \right) + \delta_0^{\gamma+\eta} \nabla_{\boldsymbol{x}} \cdot \left(\frac{|Y_t|}{|Y_c|} \kappa \boldsymbol{K} \nabla_{\boldsymbol{x}} p_t^0 \right) + \delta_1^{\gamma} \bar{R}_{\boldsymbol{n}} \frac{|\Gamma|}{|Y_c|} (p_t^0 - p_c^0) = \boldsymbol{F}_c, \tag{27a}$$

$$\chi_H(\gamma - \eta - 1) \nabla \cdot \left(\kappa \boldsymbol{K} \nabla_{\boldsymbol{x}} p_t^0 \right) - \chi_H(1 - \gamma + \eta) \bar{R}_{\boldsymbol{n}} \frac{|\Gamma|}{|Y_t|} (p_t^0 - p_c^0) = 0, \tag{27b}$$

where the tensors $\boldsymbol{K}$ and $\boldsymbol{E}$ are defined by:

$$[\boldsymbol{K}]_{ij} = \delta_{ij} - \frac{1}{|Y_t|} \int_{Y_t} \nabla_{\boldsymbol{y}} G^j \cdot \boldsymbol{e}_i \, d\, \boldsymbol{y}, \qquad [\boldsymbol{E}]_{ij} = \frac{1}{|Y_c|} \int_{Y_c} \boldsymbol{W}_j \cdot \boldsymbol{e}_i \, d\, \boldsymbol{y}, \tag{28}$$

and

$$\boldsymbol{F}_c = -\nabla \cdot (\boldsymbol{E} \boldsymbol{f}_c) \, .$$

The velocity $\boldsymbol{u}_c^\varepsilon$ and $\boldsymbol{u}_t^\varepsilon$ are then approached by

$$\boldsymbol{u}_c^\varepsilon(\boldsymbol{x}) \sim \chi_{\Omega_c^\varepsilon}(\boldsymbol{x}) \left(\boldsymbol{E} + \nabla_{\boldsymbol{y}} \underline{\mathcal{W}}(\boldsymbol{x}/\varepsilon) \right) \nabla_{\boldsymbol{x}} p_c^0(\boldsymbol{x}), \tag{29a}$$

$$\boldsymbol{u}_t^\varepsilon(\boldsymbol{x}) \sim \chi_{\Omega_t^\varepsilon}(\boldsymbol{x}) \varepsilon^\eta \bar{\kappa} \left(\boldsymbol{K} + \nabla_{\boldsymbol{y}} \underline{\mathcal{G}}(\boldsymbol{x}/\varepsilon) \right) \nabla_{\boldsymbol{x}} p_t^0(\boldsymbol{x}). \tag{29b}$$

3.4 Tensors properties

In order to ensure the well-posedness of the models that we have derived, the permeability tensors $\mathbf{K}$ and $\mathbf{E}$ need to be positive definite. This section is devoted to the analysis of the tensor properties with respect to the periodic cell Y.

Lemma 3.2. *The tensor $\boldsymbol{K}$ is symmetric and positive definite.*

Proof. Thanks to the Lax-Milgram theorem, problem (24) has a unique solution in $H^1(Y_t)/\mathbb{R}$. The variational formulation associated to (24) reads

$$\int_{Y_t} \nabla_{\mathbf{y}} \mathrm{G}^j \cdot \nabla_{\mathbf{y}} \varphi \, d\mathbf{y} - \int_{\Gamma_Y} \mathbf{e}_j \cdot \mathbf{n}_{\text{out}} \varphi \, ds = 0,$$

for any periodic $\varphi \in H^1(Y_t)$ such that $\langle \varphi \rangle_{Y_t} = 0$. Considering $\varphi = \mathrm{G}^i$ on Y_t, the following equations hold thanks to the divergence theorem

$$\begin{aligned} 0 &= \int_{Y_t} \nabla_{\mathbf{y}} \mathrm{G}^j \cdot \nabla_{\mathbf{y}} \mathrm{G}^i \, d\mathbf{y} - \int_{\Gamma_Y} \mathbf{e}_j \cdot \mathbf{n}_{\text{out}} \mathrm{G}^i \, ds \\ &= \int_{Y_t} \nabla_{\mathbf{y}} \mathrm{G}^j \cdot \nabla_{\mathbf{y}} \mathrm{G}^i \, d\mathbf{y} - \int_{Y_t} \nabla_{\mathbf{y}} \cdot \left(\mathrm{G}^i \mathbf{e}_j \right) \, d\mathbf{y} \\ &= \int_{Y_t} \nabla_{\mathbf{y}} \mathrm{G}^j \cdot \nabla_{\mathbf{y}} \mathrm{G}^i \, d\mathbf{y} - \int_{Y_t} \nabla_{\mathbf{y}} \mathrm{G}^i \cdot \mathbf{e}_j \, d\mathbf{y}. \end{aligned}$$

Therefore, the tensor $\mathbf{K}$ can be rewritten as

$$\begin{aligned} [\mathbf{K}]_{ij} &= \delta_{ij} - \frac{1}{|Y_t|} \int_{Y_t} \nabla_{\mathbf{y}} \mathrm{G}^j \cdot \mathbf{e}_i \, d\mathbf{y}, \\ &= \delta_{ij} - \frac{1}{|Y_t|} \int_{Y_t} \nabla_{\mathbf{y}} \mathrm{G}^j \cdot \nabla_{\mathbf{y}} \mathrm{G}^i \, d\mathbf{y}, \\ &= \frac{1}{Y_t} \int_{Y_t} \nabla_{\mathbf{y}} (\mathrm{G}^i - y_i) \nabla_{\mathbf{y}} (\mathrm{G}^j - y_j) \, d\mathbf{y}. \end{aligned}$$

It follows that the tensor $\mathbf{K}$ is symmetric. To prove that the tensor is positive definite, we consider any $\boldsymbol{\lambda} \in \mathbb{R}^N$ and define

$$\phi = \sum_{i=1}^{N} \lambda_i \mathrm{G}^i.$$

The function ϕ is periodic and belongs to the space $H^1(Y_t)$. We prove that $\mathbf{K}$ is semi-positive definite:

$$|Y_t| \boldsymbol{\lambda}^T \mathbf{K} \boldsymbol{\lambda} = \int_{Y_t} |\nabla_{\mathbf{y}} \left(\phi - \mathbf{y} \cdot \boldsymbol{\lambda} \right)|^2 \, d\mathbf{y} \geq 0,$$

that is true for any $\nabla_{\mathbf{y}} \left(\phi - \mathbf{y} \cdot \boldsymbol{\lambda} \right)$. The equality holds if and only if

$$\nabla_{\mathbf{y}} \phi = \boldsymbol{\lambda}.$$

However, under the assumption of periodicity in a connected domain, $\nabla_{\mathbf{y}} \phi = \boldsymbol{\lambda}$ if and only if $\nabla_{\mathbf{y}} \phi = \boldsymbol{\lambda} = \mathbf{0}$. Therefore, $\mathbf{K}$ is positive definite.

□

Remark 3.3. *The interstitial domain Y_t has to be connected to guarantee the positive*

definiteness of the tensor $\boldsymbol{K}$ *(otherwise, it is semi-positive definite).*

Lemma 3.4. *If the capillary domain* Y_c *is connected, then the tensor* $\boldsymbol{E}$ *is symmetric and positive definite.*

Proof. We proceed analogously as [4]. Thanks to the Lax-Milgram lemma, there exist a unique weak solution to problem (20), which variational formulation reads as

$$\int_{Y_c} \nu \nabla_{\mathbf{y}} \mathbf{W}^j : \nabla_{\mathbf{y}} \mathbf{v} \, d\,\mathbf{y} - \int_{Y_c} \mathbf{e}_j \cdot \mathbf{v} \, d\,\mathbf{y} = 0,$$

for any periodic $\mathbf{v} \in H^1(Y_c)$ such that $\nabla_{\mathbf{y}} \cdot \mathbf{v} = 0$ and $\mathbf{v} \cdot \mathbf{n} = 0$ on Γ_Y. Taking $\mathbf{v} = \mathbf{W}^i$ the following identity holds:

$$\begin{aligned} |Y_c|[\mathbf{E}]_{ij} &= \int_{Y_c} \mathbf{W}^j \cdot \mathbf{e}_i \, d\,\mathbf{y}, \\ &= \int_{Y_c} \nu \nabla_{\mathbf{y}} \mathbf{W}^j : \nabla_{\mathbf{y}} \mathbf{W}^i \, d\,\mathbf{y}. \end{aligned}$$

Therefore the tensor is symmetric. To prove that it is positive definite, we take any $\boldsymbol{\lambda} \in \mathbb{R}^N$ and define

$$\boldsymbol{\psi} = \sum_{i=1}^{N} \lambda_i \mathbf{W}^i.$$

We first prove that $\boldsymbol{\lambda}^T \mathbf{E} \boldsymbol{\lambda}$ is non-negative. Indeed,

$$|Y_c| \boldsymbol{\lambda}^T \mathbf{E} \boldsymbol{\lambda} = \int_{Y_c} \nu \nabla_{\mathbf{y}} \boldsymbol{\psi} : \nabla_{\mathbf{y}} \boldsymbol{\psi} \, d\,\mathbf{y} \geq 0.$$

The equality holds if and only if $\nabla_{\mathbf{y}} \boldsymbol{\psi} = 0$. Then, the following equation must be satisfied

$$\begin{aligned} &\forall \mathbf{v} \in H^1(Y_c) : \nabla_{\mathbf{y}} \cdot \mathbf{v} = 0, \\ &0 = \int_{Y_c} \nu \nabla_{\mathbf{y}} \boldsymbol{\psi} : \nabla_{\mathbf{y}} \mathbf{v} \, d\,\mathbf{y} - \int_{\Gamma_Y} \left([(\mathbf{n} \cdot \nabla_{\mathbf{y}}) \boldsymbol{\psi}] \cdot \mathbf{n} \right) (\mathbf{v} \cdot \mathbf{n}) \, d\,s = \int_{Y_c} \boldsymbol{\lambda} \cdot \mathbf{v} \, d\,\mathbf{y}, . \end{aligned} \tag{30}$$

Since (30) holds for any $\mathbf{v}$ in the appropriate space defined above, it is valid also for $\mathbf{v} = \boldsymbol{\lambda}$. Therefore, we conclude that (30) is true if and only if $\boldsymbol{\lambda} = \mathbf{0}$ and state that $\mathbf{E}$ is positive definite. □

Remark 3.5. *When the domain* Y_c *is not connected, then the unique solution to problem* (20) *is* $\boldsymbol{W}^j = \boldsymbol{0}$ *and* $P^j = y_j$*. In this case the tensor* $\boldsymbol{E}$ *is zero. If* Y_t *is not connected, then the unique solution to problem* (24) *is* $G^j = y_j$*. In this case the tensor* $\boldsymbol{K}$ *is zero.*

The fact that the effective tensor $\boldsymbol{E}$ *or* $\boldsymbol{K}$ *are zero if the corresponding phase* Y_c *or* Y_t *is not connected means that there is no long-range coupling of the pressure in the phase* Y_c *or* Y_t*. Since it is disconnected, the homogenised pressure does not satisfy an elliptic equation.*

Remark 3.6. *The tensor* $\bar{\kappa}\boldsymbol{K} + \frac{|Y_c|}{|Y_t|}\boldsymbol{E}$ *is symmetric and positive definite since it is the sum of two symmetric and positive definite tensors.*

Remark 3.7. *If one of the two domains* (Ω_c^ε *or* Ω_t^ε) *is not connected, and if* $\gamma - \eta \geq 1$ *then* $p_c = p_t$*, which means that the pressure of the disconnected phase is determined locally by the pressure of the connected phase (which satisfies an elliptic equation).*

3.5 Links between the different limit problems

We have shown that for any $(\gamma, \eta) \in \mathbb{N}^2$, the limit problems of (15) as ε goes to zero is given by (27). As shown in this section, the case $(\gamma = 1, \eta = 0)$ is the distinguished model from which the other models are derived. For large capillary permeability $\bar{R}_{\mathbf{n}}$, the tissue behaves as a monophasic material, and the question of appropriate boundary condition is adressed at the end of the section.

In this section, we show the link between the different models. We assume that both instertitium and capillary phases are connected so that both $\mathbf{E}$ and $\mathbf{K}$ are postive definite and the problem (27) complemented with Dirichlet, Neumann or Robin-Fourier conditions is well-posed.

Passing from the case $(\gamma = 1, \eta = 0)$ **to** $(\gamma \geq 2, \gamma - \eta \geq 1)$

Consider the limit model in the case $(\gamma = 1, \eta = 0)$. According to (27), it reads

$$\nabla \cdot (\bar{\kappa}\mathbf{K}\nabla p_t) = \frac{\bar{R}_{\mathbf{n}}|\Gamma_Y|}{|Y_t|}(p_t - p_c) \qquad \text{in } \Omega, \tag{31a}$$

$$\nabla \cdot (\mathbf{E}\nabla p_c) = \frac{\bar{R}_{\mathbf{n}}|\Gamma_Y|}{|Y_c|}(p_c - p_t) \qquad \text{in } \Omega, \tag{31b}$$

$$p_t|_{\partial\Omega} = p_{t,\infty}, \qquad p_c|_{\partial\Omega} = p_{c,\infty}, \qquad \text{on } \partial\Omega. \tag{31c}$$

Consider now that $\bar{\kappa} = \varepsilon^a\tilde{\kappa}$ and $\bar{R}_{\mathbf{n}} = \varepsilon^b\tilde{R}_{\mathbf{n}}$, with $b - a \geq 0$ and $b > 0$. It is clear that (31b) is not a singluar perturbation of the operator $\nabla \cdot (\mathbf{E}\nabla\cdot)$ in the sense of Kato [29] and thus the solution to problem (31) tends to the solution to the following problem, which is nothing that model $\gamma - \eta = 1 + a - b \geq 1$ with $\gamma > 1$:

$$\nabla \cdot (\tilde{\kappa}\mathbf{K}\nabla p_t) = \delta_0^{b-a}\frac{\tilde{R}_{\mathbf{n}}|\Gamma_Y|}{|Y_t|}(p_t - p_c) \qquad \text{in } \Omega,$$

$$\nabla \cdot (\mathbf{E}\nabla p_c) = 0 \qquad \text{in } \Omega,$$

$$p_t|_{\partial\Omega} = p_{t,\infty}, \qquad p_c|_{\partial\Omega} = p_{c,\infty}, \qquad \text{on } \partial\Omega.$$

Passing from the case $(\gamma = 1, \eta = 0)$ **to** $(\gamma = 0, \eta = 0)$

Considering $\bar{R}_{\mathbf{n}}$ of the order of ε^{-1} and $\bar{\kappa}$ of the order of 1, model $(\gamma = 1, \eta = 0)$ reads then

$$\varepsilon \nabla \cdot (\tilde{\kappa} \mathbf{K} \nabla p_t) = \frac{\tilde{R}_{\mathbf{n}} |\Gamma_Y|}{|Y_t|} (p_t - p_c) \qquad \text{in } \Omega, \tag{32a}$$

$$\varepsilon \nabla \cdot (\mathbf{E} \nabla p_c) = \frac{\tilde{R}_{\mathbf{n}} |\Gamma_Y|}{|Y_c|} (p_c - p_t) \qquad \text{in } \Omega \tag{32b}$$

$$p_t|_{\partial\Omega} = p_{t,\infty}, \qquad p_c|_{\partial\Omega} = p_{c,\infty}, \qquad \text{on } \partial\Omega. \tag{32c}$$

Here the asymptotic analysis is much trickier since both equations (32a)–(32b) are singular perturbation of the div-grad operator. In particular, a delicate asymptotic analysis makes appear a exponential decay of the $p_t - p_c$ from the boundary, showing that out of the vicinity of the tumor boundary, both pressures are equal. The details of this results are given in [55], however we expose here the main arguments in the simple case where $\bar{\kappa}\mathbf{K}$ and $\mathbf{E}$ are colinear to the identity, that is for a $\lambda \neq 0$:

$$\bar{\kappa}\mathbf{K} = \lambda \mathbf{E}$$

Then simple calculation shows that

$$\nabla \cdot (\mathbf{E} \nabla (p_t - p_c)) = \frac{\bar{R}_{\mathbf{n}}}{\varepsilon} \left(\frac{|\Gamma_Y|}{\lambda |Y_t|} + \frac{|\Gamma_Y|}{|Y_c|} \right) (p_t - p_c) \qquad \text{in } \Omega, \tag{33}$$

It is well-known, especially in conduction theory [7, 20] that problem (33) makes appear a so-called skin depth effect: the pressure difference $p_t - p_c$ decays exponentially fast from the boundary. More precisely, denoting by α the factor given by

$$\alpha = \sqrt{\bar{R}_{\mathbf{n}} \left(\frac{|\Gamma_Y|}{\lambda |Y_t|} + \frac{|\Gamma_Y|}{|Y_c|} \right)},$$

hence in the local coordinates near the boundary

$$p_t - p_c = (p_{t,\infty} - p_{c,\infty}) e^{-\frac{\alpha}{\sqrt{\varepsilon}} x_n} + o(\varepsilon),$$

where x_n is the normal variable with respect to the tumor boundary.

Interestingly, we thus obtain that in this asymptotic regime, the solution to model $(\gamma = 1, \eta = 0)$ with Dirichlet boundary conditions can be approached by the solution to model $(\gamma = 0, \eta = 0)$ with the following appropriate boundary condition

$$\nabla \cdot ((\lambda + 1) \mathbf{E} \nabla p) = 0, \qquad \text{in } \Omega$$

$$p|_{\partial\Omega} = \frac{1}{2} (p_{t,\infty} + p_{c,\infty}) - \frac{|Y_c| - \lambda |Y_t|}{|Y_c| + \lambda |Y_t|} \frac{1}{2} (p_{t,\infty} - p_{c,\infty}), \qquad \text{on } \partial\Omega.$$

The rigorous proof is provided in [55]. The result involves Riemannian geometry results which are far from the scope of this paper, however the general idea of the exponential decay of the pressure difference remains.

4 Numerical simulations

The Galerkin Finite Elements Method was used to discretize the equations in order to test the homogenized models. The 3 following cases are considered : $(\gamma = 0, \eta = 0)$, $(\gamma = 1, \eta = 0)$, $(\gamma = 2, \eta = 1)$. 3D simulations were run in order to analyse the impact of the micro-scale geometry on the homogenized solutions and the influence of the vessel permeability $R_{\mathbf{n}}$ on the fluid transport. The following strategy has been adopted:

- The periodic cell was considered as the unit cube $(0,1)^3$ in $\mathbb{R}^3$. The domain was divided in two regions (Y_t and Y_c) and the software `Gmsh` was used to perform the triangulation $\mathcal{T}_h$. Problem (20) was discretized with the Galerkin Finite Elements Method. Piecewise linear polynomials ($\mathbb{P}_1$) were used for the variable P^j. For the variable $\mathbf{W}^j$, we used piecewise linear polynomials with bubbles ($\mathbb{P}_{1b} = \{v \in H^1(\Omega) : \forall K \in \mathcal{T}_h \quad v|_K \in \mathbb{P}_1 \oplus \mathrm{Span}\{\lambda_0^K \lambda_1^K \lambda_2^K \lambda_3^K\}\}$, where $\lambda_j^K, j = 0, ..., N$ are the 4 barycentric coordinate functions of the element K). Problem (24) was solved on the domain Y_t using piecewise linear polynomials ($\mathbb{P}_1$) for the variable G^j.
- The tensors $\mathbf{K}$ and $\mathbf{E}$ were computed according to (28).
- The homogenized model (27) for the three cases $(\gamma = 0, \eta = 0)$, $(\gamma = 1, \eta = 0)$, $(\gamma = 2, \eta = 1)$ was simulated on the normalized sphere of radius 0.5 using the Galerkin Finite Elements Method. Quadratic piecewise elements ($\mathbb{P}_2$) were used for both p_t and p_c.

4.1 Cell problems: tensor properties varying the microstructure

The tensors $\mathbf{K}$ and $\mathbf{E}$ defined in (28) have different properties according to the microstructure. To analyse them, we solved equations (24) and (20) in the unitary cell, i.e. the cube $(0,1)^3 \subset \mathbb{R}^3$. Different geometric configurations for the domains Y_t and Y_c were tested (Figure 3).

Table 1 provides the values of the elements in the two tensors $\mathbf{K}$ and $\mathbf{E}$. These results confirm the analysis done in Section 3.4. Indeed, the tensors $\mathbf{K}$ and $\mathbf{E}$ are symmetric and positive definite when the two domains are connected (Fig. 3a, 3b and 3c). When the capillaries are not connected in all the directions (Fig. 3d, 3e), the tensor $\mathbf{E}$ is semi-positive definite as the solution to the cell problems (24) is trivial: $\mathbf{W}^j = 0$ and $\mathrm{P}^j = \mathbf{e}_j$, $j = 1, 2, 3$. Figure 3 provides the values of the interstitial and capillary volume fractions ($|Y_t|$ and $|Y_c|$, respectively) and of the vascular surface Γ_Y.

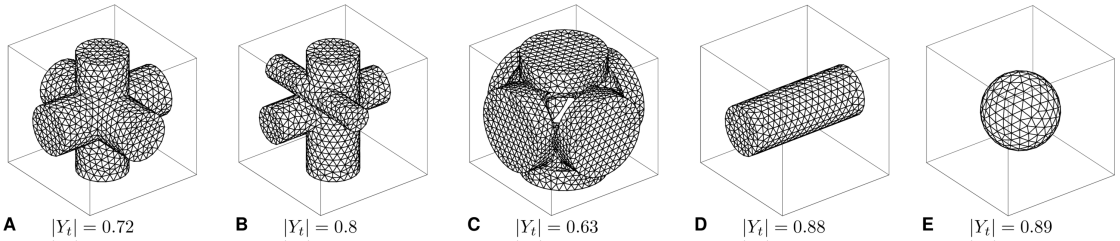

Figure 3. Different structures of the unit periodic cell with the respective volume and surface fractions. The mesh represents the capillary domain Y_c, while the difference between the box and the mesh is the interstitial compartment Y_t.

	$\mathbf{K}_{11}$	$\mathbf{K}_{12}$	$\mathbf{K}_{13}$	$\mathbf{K}_{21}$	$\mathbf{K}_{22}$	$\mathbf{K}_{23}$	$\mathbf{K}_{31}$	$\mathbf{K}_{32}$	$\mathbf{K}_{33}$
Fig 3a	0.808	7.5e-5	7.89e-6	7.5e-5	0.808	5.49e-5	7.89e-6	5.49e-5	0.808
Fig 3b	0.877	-1.76e-3	3.91e-3	-1.76e-3	0.814	2.29e-3	3.91e-3	2.29e-3	0.933
Fig 3c	0.72	-1.09e-4	1.03e-4	-1.09e-4	0.72	3.98e-5	1.03e-4	3.98e-5	0.72
Fig 3d	1	-3.19e-8	-9.81e-8	-3.19e-8	0.895	1.01e-4	-9.81e-8	1.01e-4	0.895
Fig 3e	0.954	-4.69e-5	5.2e-5	-4.69e-5	0.954	8.14e-5	5.2e-5	8.14e-5	0.954

	$\mathbf{E}_{11}$	$\mathbf{E}_{12}$	$\mathbf{E}_{13}$	$\mathbf{E}_{21}$	$\mathbf{E}_{22}$	$\mathbf{E}_{23}$	$\mathbf{E}_{31}$	$\mathbf{E}_{32}$	$\mathbf{E}_{33}$
Fig 3a	2.2e-3	8e-6	-1.1e-6	8e-6	2.2e-3	-1.3e-5	-1.1e-6	-1.3e-5	2.2e-3
Fig 3b	9.5e-4	8.1e-7	2.3e-5	8.1e-7	1.8e-4	7.7e-6	2.3e-5	7.7e-6	2.9e-3
Fig 3c	4.0e-4	-8.7e-7	-7.4e-7	-8.7e-7	4.0e-4	-2.7e-6	-7.4e-7	-2.7e-6	4.0e-4
Fig 3d	4.7e-3	0	0	0	0	0	0	0	0
Fig 3e	0	0	0	0	0	0	0	0	0

Table 1. Values of the tensors **K** and **E** for the different microstructures depicted in Fig. 3.

4.2 Macroscopic dynamic of fluid transport in tumours

We eventually considered realistic parameters to test model (2). The homogenized model was tested with a tumor considered as a sphere of normalized radius 0.5. Table 2 provides the values of the parameters of the model. Regarding the interstitial hydraulic conductivity k_t, the vascular permeability L_p and the tumour characteristic length L, we considered values relative to different tissues, as summarized in Tables 3, 4 and 5, respectively. Simulations were run considering different microstructures, namely the ones shown in Figs 3a-c. Dirichlet boundary conditions were considered for the interstitial and capillary pressure, specifically $p_{t,\infty} = 0$ and $p_{c,\infty} = 1$ (normalized values).

Parameter influence

First, we looked at the behaviour of the solution varying the parameters k_t, L_p and L. Examples of solutions as a function of the radius are shown in Fig. 4. In this case, we considered the microstructure of Fig. 3c. Results relative to the interstitial pressure and velocity were in agreement with the ones found in [9], where the authors considered the following model:

$$\nabla \cdot (\mathbf{K} \nabla p_t) = \frac{\bar{R}_{\mathbf{n}} S}{\bar{\kappa} V} (p_t - p_c), \tag{34}$$

where the vascular pressure p_c is assumed to be constant and S/V is the vascular area per unit volume of the tumour. Therefore, we considered this value to be equal to $|\Gamma_Y|$. The slight differences between the results obtained from the homogenized model and Baxter and Jain model (34) (Figure 4A) are due to the different rescaling of the equation, since we considered S/V to be the vascular area per unit volume of the interstitial compartment ($|\Gamma_Y|/|Y_t|$).

The interstitial fluid pressure is large and almost constant in the centre of the tumour and has a sharp drop at the periphery for increasing values of $\bar{R}_{\mathbf{n}}$ and decrasing values of $\bar{\kappa}$. As a consequence, the interstitial fluid velocity is almost zero in the centre of the tumour (since the pressure gradient is close to zero) and large at the periphery. The microvessel fluid pressure is almost constant and close to the value at the boundary. For large values of the parameter $\bar{R}_{\mathbf{n}}$, the capillary pressure decreases and gets closer to the interstitial fluid pressure. As a consequence, also the microvessel fluid velocity is close to zero in the centre of the tumour.

Eventually, we observed the skin depth effect of $p_c - p_t$ when the permeability of the vessel walls increases (Fig 4B). Indeed, the pressure difference is almost zero at the centre of the tumour and increases exponentially in correspondence of the boundary.

Microstructure

We fixed the parameter values $k_t = 1.8 \cdot 10^{-12}$ m$^3\cdot$ s $\cdot$ kg^{-1}, $L_p = 1.86 \cdot 10^{-10}$ m$^2\cdot$ s $\cdot$ kg^{-1} and $L = 5$ mm and looked at the behaviour of the solutions relative to the different microstructures. Fig. 5 shows the results relative to the unitary cells of Fig 3A-C. In all cases, the IFP shows a sharp drop at the periphery and it equates the capillary pressure in the centre of the tumour, while the capillary pressure is approximately constant in the whole tumour. The interstitial fluid velocity $\mathbf{u}_t$ is directed outward from the domain, while the blood velocity is directed inward. The two velocities are radially homogeneous in cases 5A and 5C, while they show asymmetries in case 5B due to the asymmetric microscopic structure of Fig 3B.

We noticed that only when the capillary subdomain is smaller than the interstitial region, the blood velocity is larger than the interstitial fluid flow (data not shown). This is biologically relevant as the capillary volume fraction is usually within the range [16%, 50%] [18] and the average blood velocity is larger than the interstitial fluid velocity [58, 27].

Boundary conditions

Eventually, we tested model (2) with different boundary conditions. In particular, Neumann boundary conditions were considered for the capillary pressure, in order to ensure the continuity of the normal velocity in the vessels at the tumour periphery:

$$-\mathbf{E}\nabla p_c \cdot \mathbf{n} = \mathbf{u}_{c,\infty} \cdot \mathbf{n},$$

where $\mathbf{u}_{c,\infty}$ is the blood velocity in the sourranding tissue. Dirichlet boundary conditions were imposed to the interstitial pressure. Well-posedness of model (2) is guaranteed with this set of boundary conditions for $(p_t, p_c) \in H_0^1(\Omega) \times H^1(\Omega)$.

We ran experiments with different boundary conditions for the capillary pressure p_c as summarized in Table 6. Homogeneous Dirichlet boundary conditions were considered for the interstitial fluid pressure p_t. Figure S1 shows the results at the centre of the sphere as function of the normalized radius. The interstitial pressure increases at the centre of the tumour and equates the blood pressure in the three cases. When considering the case "Neumann 2", the blood velocity is constantly high inside the domain and the capillary pressure profile is therefore due to the gradient along the x-axis.

5 Discussion

We have provided an analysis of the impact of microstructure properties of the tumour employing the homogenisation theory.
First, we have described a model at the microscopic scale that couples vascular, transvascular and interstitial fluids, adopting an asymptotic expansion technique. Then, we have

Parameter	Description	Value	Unit	Reference
μ	blood viscosity	$4 \cdot 10^{-3}$	$\mathrm{kg} \cdot \mathrm{m}^{-1} \cdot \mathrm{s}^{-1}$	[42]
d	mean intercapillary distance	$50 \cdot 10^{-6}$	m	[32]
α_{BJ}	BJS constant	1	-	-
$p_{t,\infty}$	surrounding interstitial pressure	0	mmHg	-
$p_{c,\infty}$	surrounding capillary pressure	[15,80]	mmHg	[13]

Table 2. Fixed parameters used to simulate IFP and IFV.

Tissue	k_t $[\mathrm{m}^3 \cdot \mathrm{s} \cdot \mathrm{kg}^{-1}]$	Reference
Dog squamous cell tissue	$1.8 \cdot 10^{-12}$	[19]
Mouse mammary carcinoma	$1.88 \cdot 10^{-13}$	[26]
Hepatoma 5123 in vivo	$2.9 \cdot 10^{-15}$	[53]

Table 3. Values of the interstitial hydraulic conductivity k_t of different tissues.

Tissue	L_p $[\mathrm{m}^2 \cdot \mathrm{s} \cdot \mathrm{kg}^{-1}]$	Reference
Mouse mammary carcinoma	$1.86 \cdot 10^{-10}$	[26]
R3230 mammary adenocarcinoma	$4.5 \cdot 10^{-11}$	[47]
Healty rat hindquarter tissue	$2.3 \cdot 10^{-12}$	[43]

Table 4. Values of the vessel permeability L_p of different tissues.

Characteristic length L [mm]	Tumor volume $[\mathrm{mm}^3]$	$\varepsilon = d/L$
5	4.2	0.05
10	523.6	0.01
15	4200	0.005

Table 5. Characteristic length (diameter) of the tumour and corresponding tumour volume and value of ε.

Experiment	Boundary condition (on $\partial\Omega$)	Parameter value (normalized)
Dirichlet	$p_c = p_{c,\infty}$	$p_{c,\infty} = 1$
Neumann 1	$-\mathbf{E}\nabla p_c \cdot \mathbf{n} = \mathbf{u}_{c,\infty} \cdot \mathbf{n}$	$\mathbf{u}_{c,\infty} = -1 \cdot 10^{-3}\mathbf{n}$
Neumann 2	$-\mathbf{E}\nabla p_c \cdot \mathbf{n} = \mathbf{u}_{c,\infty} \cdot \mathbf{n}$	$\mathbf{u}_{c,\infty} = [-1 \cdot 10^{-5}, 0, 0]^T$

Table 6. Different boundary conditions considered for the microvessel pressure p_c.

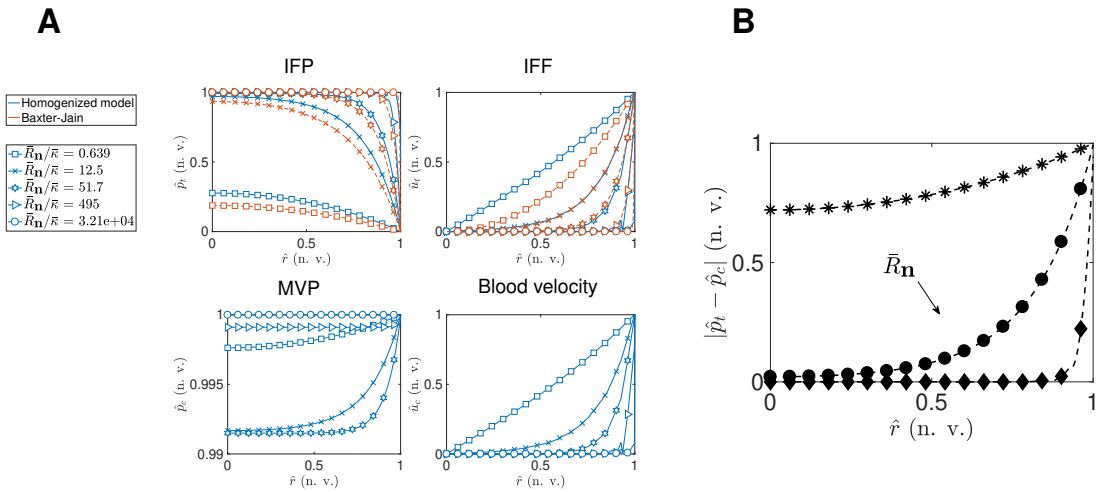

Figure 4. (A) Normalized values (n.v.) of interstitial fluid pressure and flow (IFP and IFF), of microvascular pressure (MVP) and of blood velocity as functions of the normalized radius $\hat{r}$ varying the parameter $\bar{R}_{\mathbf{n}}/\kappa$. The microstructure considered in this case corresponds to Fig 3c. The blue lines are the simulations of the homogenized model (2) and the red lines are the results of Baxter and Jain model [9]. (B) Difference between $\hat{p}_c$ and $\hat{p}_t$ in normalized values (n.v.) as functions of the normalized radius $\hat{r}$ varying the parameter $\bar{R}_{\mathbf{n}}$ and with $\bar{\kappa}$ fixed.

derived three macro-scale models according to the vessel wall permeability and the interstitial hydraulic conductivity. After having analysed the well-posedness of the problems, we performed numerical simulations to assess some properties according to the microstructure.

Well-posedness is guaranteed when the two subdomains Y_t and Y_c are connected. When one region is not connected with respect to one axis, the fluid is not transported along this direction. For example, in Fig. 3e the capillary microstructure is a closed sphere, therefore there is no fluid transport in the blood vessels; in Fig. 3d, the vessel geometry is connected only along the x-axis that is the only direction for the capillary fluid flow. This represents a limit for the 2D simulations, as the subdomains Y_t and Y_c cannot be both connected. In this case, one among the interstitial or the vessel flow is always zero. However, tensors $\mathbf{K}$ and $\mathbf{E}$ can be determined by calibrating directly the homogenized models to medical imaging data.

Furthermore, we motivated the links between the various regimes and shown that model (2) covers a wide range of cases, confirming previous results [48]. In particular, we have shown that model (1) is equivalent to model (2) under certain conditions and that model (2) can be approximated to model (3) under certain assumptions on the parameters.

Eventually, we calibrated model (2) with parameters taken from the literature and

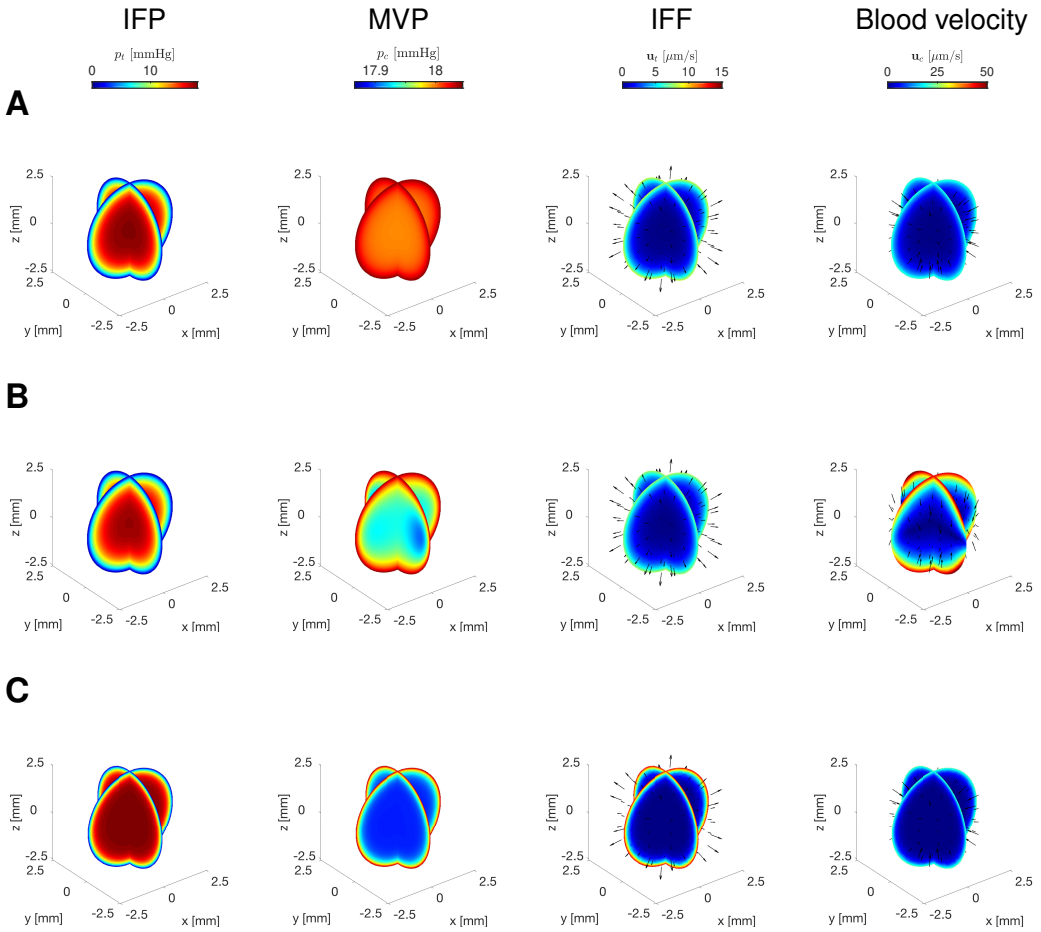

Figure 5. 3D slices at the centre of the sphere with the interstitial pressure (first column), the capillary pressure (second comumn), interstitial velocity (third column) and capillary velocity (fourth column). Results were computed using the microstructure of Fig 3a (A), of Fig 3b (B) and of Fig 3c (C) and setting $k_t = 1.8 \cdot 10^{-12}$ m$^3 \cdot$ s $\cdot$ kg^{-1}, $L_p = 1.86 \cdot 10^{-10}$ m$^2 \cdot$ s $\cdot$ kg^{-1} and $L = 5$ mm. IFP = interstitial fluid pressure, MVP = microvascular pressure, IFF = interstitial fluid flow.

analysed their influence on the solutions. We observed that different microstructures and different sets of boundary conditions strongly impact the macroscopic dynamics of the fluids. The geometric shape of the unitary cell influences the isotropy of the capillary fluid velocity, while the vascular volume fraction affects the blood velocity. Indeed, when the capillary volume fraction $|Y_c|$ is large, the blood velocity $\mathbf{u}_c$ is equal or lower than the interstitial fluid velocity $\mathbf{u}_t$. This might not be biologically relevant. On the other hand, when the capillary volume fraction is smaller the blood velocity is of higher magnitude and gets closer to the average values (around 1.62 mm $\cdot$ s^{-1} [51]). This confirms that the homogenized models are consistent with biological observations. Indeed, the vascular volume fraction lies within the values of 16% and 50%. [18, 22, 56]. Moreover, the average values of the pressures and of the velocities obtained from simulations with different sets of boundary conditions were compared against literature values. When Dirichlet-Dirichlet boundary conditions are considered, both the interstitial and the capillary pressures fit better the well-known profile of the IFP that is high at the centre of the tumour and shows a sharp drop at the periphery [9]. However, when Dirichlet-Neumann boundary conditions are considered for the interstitial and the capillary pressure, respectively, the blood velocity reaches average values closer to the literature ones. Possible improvements of our computations might be achieved by considering the correctors and by adding boundary layers, to take into account the Dirichlet boundary conditions that are imposed to the true solution $(p_t^\varepsilon, p_c^\varepsilon)$ of the micro-scale model, but are not satisfied by the periodic solutions to the homogenized ones.

The current work focuses on the analysis of asymptotic models that describe fluid transport in tumour tissues. Fluid velocities are necessary to develop convection-diffusion models for the description of drug transport in tumour tissues. This motivated our choice of a steady-state model, as in reality, the time variation of the fluid transport is negligible with respect to the evolution of drug distribution inside the tumour. However, spatial tumour growth might be included in the model.
Further extensions might include a relaxation of the periodicity hypothesis, that might not be realistic in a biological context, as tumours are highly heterogeneous. This question is complex and few results have been obtained in these directions. Actually, the current results on stochastic homogenisation are proven under an ergodic assumption which states that the domain is somehow almost invariant under a specific translation. This assumption enables to define properly a representative volume element, which the stochastic equivalent to the periodic unit cell. The homogenisation correctors $\underline{\mathcal{W}}, \mathcal{P}, \mathcal{G}$ can then be computed in this representative volume, enabling the computation of the effective tensors $\mathbf{E}$ and $\mathbf{K}$[28].

Moreover, rheological effects of blood should be included to model blood transport in capillaries [41].

Applications of the models include the incorporation of 3D imaging data. Images provide the microstructure of the vessel network, that is necesssary to compute the correctors.

References

[1] G. Allaire. Homogenization and Two-Scale Convergence. *SIAM J. Math. Anal.*, 23(6):1482–1518, Nov. 1992.

[2] M. Amar, D. Andreucci, P. Bisegna, and R. Gianni. On a hierarchy of models for electrical conduction in biological tissues. *Math. Meth. Appl. Sci.*, 29(7):767–787, May 2006.

[3] A. Apelblat, A. Katzir-Katchalsky, and A. Silberberg. A mathematical analysis of capillary-tissue fluid exchange. *Biorheology*, 11(1):1–49, Feb. 1974.

[4] T. Arbogast and H. L. Lehr. Homogenization of a Darcy–Stokes system modeling vuggy porous media. *Comput. Geosci.*, 10(3):291–302, Sept. 2006.

[5] J. W. Baish, Y. Gazit, D. A. Berk, M. Nozue, L. T. Baxter, and R. K. Jain. Role of tumor vascular architecture in nutrient and drug delivery: An invasion percolation-based network model. *Microvasc. Res.*, 51(3):327–346, May 1996.

[6] J. W. Baish, P. A. Netti, and R. K. Jain. Transmural coupling of fluid flow in microcirculatory network and interstitium in tumors. *Microvasc. Res.*, 53(2):128–141, Mar. 1997.

[7] C. A. Balanis. *Advanced Engineering Electromagnetics*. John Wiley & Sons, Hoboken, N.J, 2nd ed edition, 2012.

[8] K. Bartha and H. Rieger. Vascular network remodeling via vessel cooption, regression and growth in tumors. *J. Theor. Biol*, 241(4):903–918, Aug. 2006.

[9] L. T. Baxter and R. K. Jain. Transport of fluid and macromolecules in tumors. I. Role of interstitial pressure and convection. *Microvasc. Res.*, 37(1):77–104, Jan. 1989.

[10] G. S. Beavers and D. D. Joseph. Boundary conditions at a naturally permeable wall. *J. Fluid. Mech*, 30(1):197–207, Oct. 1967.

[11] T. R. Blake and J. F. Gross. Analysis of coupled intra- and extraluminal flows for single and multiple capillaries. *Math. Biosci.*, 59(2):173–206, June 1982.

[12] Y. Boucher, L. T. Baxter, and R. K. Jain. Interstitial pressure gradients in tissue-isolated and subcutaneous tumors: Implications for therapy. *Cancer Res.*, 50(15):4478–4484, Aug. 1990.

[13] Y. Boucher and R. K. Jain. Microvascular pressure is the principal driving force for interstitial hypertension in solid tumors: Implications for vascular collapse. *Cancer Res.*, 52(18):5110–5114, Sept. 1992.

[14] V. P. Chauhan, T. Stylianopoulos, Y. Boucher, and R. K. Jain. Delivery of Molecular and Nanoscale Medicine to Tumors: Transport Barriers and Strategies. *Annu. Rev. Chem. Biomol. Eng.*, 2(1):281–298, July 2011.

[15] C. Conca. On the application of the homogenization theory to a class of problems arising in fluid mechanics. *J. Math. Pures Appl.*, 64:31–75, 1985.

[16] M. Discacciati and A. Quarteroni. Navier-Stokes/darcy coupling: Modeling, analysis, and numerical approximation. *Rev. Mat. Complut.*, 22(2), July 2009.

[17] H. F. Dvorak, L. F. Brown, M. Detmar, and A. M. Dvorak. Vascular permeability factor/vascular endothelial growth factor, microvascular hyperpermeability, and angiogenesis. *Am. J. Pathol.*, 146(5):1029–1039, May 1995.

[18] J. C. Forster, W. M. Harriss-Phillips, M. J. Douglass, and E. Bezak. A review of the development of tumor vasculature and its effects on the tumor microenvironment. *Hypoxia (Auckl)*, 5:21–32, 2017.

[19] A. C. Guyton, H. J. Granger, and A. E. Taylor. Interstitial fluid pressure. *Physiol Rev.*, 51(3):527–563, July 1971.

[20] H. Haddar, P. Joly, and H.-M. Nguyen. Generalized Impedance Impedance Boundary Conditions For Scattering by Strongly Absorbing Obstacles: The Scalar Case. *Math. Models Methods Appl. Sci.*, 15(08):1273–1300, Aug. 2005.

[21] G. Helmlinger, P. A. Netti, H. C. Lichtenbeld, R. J. Melder, and R. K. Jain. Solid stress inhibits the growth of multicellular tumor spheroids. *Nat Biotechnol*, 15(8):778–783, Aug. 1997.

[22] D. E. Hilmas and E. L. Gillette. Morphometric analyses of the microvasculature of tumors during growth and after x-irradiation. *Cancer*, 33(1):103–110, Jan. 1974.

[23] R. K. Jain. Transport of molecules in the tumor interstitium: A review. *Cancer Res.*, 47(12):3039–3051, June 1987.

[24] R. K. Jain. Barriers to drug delivery in solid tumors. *Sci. Am.*, 271(1):58–65, July 1994.

[25] R. K. Jain and L. T. Baxter. Mechanisms of heterogeneous distribution of monoclonal antibodies and other macromolecules in tumors: Significance of elevated interstitial pressure. *Cancer Res.*, 48(24 Pt 1):7022–7032, Dec. 1988.

[26] R. K. Jain, R. T. Tong, and L. L. Munn. Effect of Vascular Normalization by Antiangiogenic Therapy on Interstitial Hypertension, Peritumor Edema, and Lymphatic Metastasis: Insights from a Mathematical Model. *Cancer Res.*, 67(6):2729–2735, Mar. 2007.

[27] W. S. Kamoun, S.-S. Chae, D. A. Lacorre, J. A. Tyrrell, M. Mitre, M. A. Gillissen, D. Fukumura, R. K. Jain, and L. L. Munn. Simultaneous measurement of RBC velocity, flux, hematocrit and shear rate in vascular networks. *Nat. Methods*, 7(8):655–660, Aug. 2010.

[28] T. Kanit, S. Forest, I. Galliet, V. Mounoury, and D. Jeulin. Determination of the size of the representative volume element for random composites: Statistical and numerical approach. *Int J Solids Struct*, 40(13-14):3647–3679, June 2003.

[29] T. Kato. *Perturbation Theory for Linear Operators*, volume 132 of *Classics in Mathematics*. Springer Berlin Heidelberg, Berlin, Heidelberg, 1995.

[30] A. Krogh. *The Anatomy and Physiology of Capillaries*. New Haven, Yale Univ. Press, 1922.

[31] W. J. Layton, F. Schieweck, and I. Yotov. Coupling Fluid Flow with Porous Media Flow. *SIAM J. Numer. Anal.*, 40(6):2195–2218, Jan. 2002.

[32] J. R. Less, T. C. Skalak, E. M. Sevick, and R. K. Jain. Microvascular architecture in a mammary carcinoma: Branching patterns and vessel dimensions. *Cancer Res.*, 51(1):265–273, Jan. 1991.

[33] P. A. Netti, L. T. Baxter, Y. Boucher, R. Skalak, and R. K. Jain. Time-dependent behavior of interstitial fluid pressure in solid tumors: Implications for drug delivery. *Cancer Res.*, 55(22):5451–5458, Nov. 1995.

[34] P. A. Netti, D. A. Berk, M. A. Swartz, A. J. Grodzinsky, and R. K. Jain. Role of extracellular matrix assembly in interstitial transport in solid tumors. *Cancer Res.*, 60(9):2497–2503, May 2000.

[35] M. R. Owen, T. Alarcón, P. K. Maini, and H. M. Byrne. Angiogenesis and vascular remodelling in normal and cancerous tissues. *J Math Biol*, 58(4-5):689–721, Apr. 2009.

[36] R. Penta, D. Ambrosi, and A. Quarteroni. Multiscale homogenization for fluid and drug transport in vascularized malignant tissues. *Math. Models Methods Appl. Sci.*, 25(01):79–108, Jan. 2015.

[37] R. Penta, D. Ambrosi, and R. J. Shipley. Effective governing equations for poroelastic growing media. *Q. J. Mech. Appl. Math.*, 67(1):69–91, Feb. 2014.

[38] R. Penta and J. Merodio. Homogenized modeling for vascularized poroelastic materials. *Meccanica*, 52(14):3321–3343, Nov. 2017.

[39] R. Perrussel and C. Poignard. Asymptotic expansion of steady-state potential in a high contrast medium with a thin resistive layer. *Appl Math Comput*, 221:48–65, Sept. 2013.

[40] C. Pozrikidis and D. A. Farrow. A Model of Fluid Flow in Solid Tumors. *Ann Biomed Eng*, 31(2):181–194, Feb. 2003.

[41] A. R. Pries, T. W. Secomb, T. Gessner, M. B. Sperandio, J. F. Gross, and P. Gaehtgens. Resistance to blood flow in microvessels in vivo. *Circ Res*, 75(5):904–915, Nov. 1994.

[42] P. W. Rand, E. Lacombe, H. E. Hunt, and W. H. Austin. Viscosity of normal human blood under normothermic and hypothermic conditions. *J. Appl. Physiol.*, 19(1):117–122, Jan. 1964.

[43] B. Rippe, A. Kamiya, and B. Folkow. Simultaneous measurements of capillary diffusion and filtration exchange during shifts in filtration-absorption and at graded alterations in the capillary permeability surface area product (PS). *Acta Physiol. Scand.*, 104(3):318–336, Nov. 1978.

[44] P. G. Saffman. On the Boundary Condition at the Surface of a Porous Medium. *Stud. Appl. Math.*, 50(2):93–101, June 1971.

[45] M. M. Schuff, J. P. Gore, and E. A. Nauman. A mixture theory model of fluid and solute transport in the microvasculature of normal and malignant tissues. I. Theory. *J Math Biol*, 66(6):1179–1207, May 2013.

[46] E. M. Sevick and R. K. Jain. Viscous resistance to blood flow in solid tumors: Effect of hematocrit on intratumor blood viscosity. *Cancer Res.*, 49(13):3513–3519, July 1989.

[47] E. M. Sevick and R. K. Jain. Measurement of capillary filtration coefficient in a solid tumor. *Cancer Res.*, 51(4):1352–1355, Feb. 1991.

[48] R. J. Shipley and S. J. Chapman. Multiscale Modelling of Fluid and Drug Transport in Vascular Tumours. *Bull Math Biol*, 72(6):1464–1491, Aug. 2010.

[49] R. J. Shipley, P. W. Sweeney, S. J. Chapman, and T. Roose. A four-compartment multiscale model of fluid and drug distribution in vascular tumours. *Int J Numer Method Biomed Eng*, Feb. 2020.

[50] M. Soltani and P. Chen. Numerical Modeling of Fluid Flow in Solid Tumors. *PLoS ONE*, 6(6):e20344, June 2011.

[51] S. K. Stamatelos, E. Kim, A. P. Pathak, and A. S. Popel. A bioimage informatics based reconstruction of breast tumor microvasculature with computational blood flow predictions. *Microvasc. Res.*, 91:8–21, Jan. 2014.

[52] E. H. Starling. On the Absorption of Fluids from the Connective Tissue Spaces. *J Physiol*, 19(4):312–326, May 1896.

[53] E. A. Swabb, J. Wei, and P. M. Gullino. Diffusion and convection in normal and neoplastic tissues. *Cancer Res.*, 34(10):2814–2822, Oct. 1974.

[54] P. W. Sweeney, A. d'Esposito, S. Walker-Samuel, and R. J. Shipley. Modelling the transport of fluid through heterogeneous, whole tumours in silico. *PLoS Comput Biol*, 15(6):e1006751, June 2019.

[55] C. Vaghi, S. Benzekry, and C. Poignard. Asymptotic analysis of a biphase tumor fluid flow: the weak coupling case. *Applied Mathematics and Computation*, 413:126635, 2022.

[56] A. W. Vogel. Intratumoral Vascular Changes With Increased Size of a Mammary Adenocarcinoma: New Method and Results. *J. Natl. Cancer Inst.*, 34:571–578, May 1965.

[57] C. Voutouri and T. Stylianopoulos. Evolution of osmotic pressure in solid tumors. *J Biomech.*, 47(14):3441–3447, Nov. 2014.

[58] S. Walker-Samuel, T. A. Roberts, R. Ramasawmy, J. S. Burrell, S. P. Johnson, B. M. Siow, S. Richardson, M. R. Gonçalves, D. Pendse, S. P. Robinson, R. B. Pedley, and M. F. Lythgoe. Investigating Low-Velocity Fluid Flow in Tumors with Convection-MRI. *Cancer Res*, 78(7):1859–1872, Apr. 2018.

[59] M. Welter and H. Rieger. Interstitial fluid flow and drug delivery in vascularized tumors: A computational model. *PLoS ONE*, 8(8):e70395, 2013.

[60] P. A. Wijeratne, J. H. Hipwell, D. J. Hawkes, T. Stylianopoulos, and V. Vavourakis. Multiscale biphasic modelling of peritumoural collagen microstructure: The effect of tumour growth on permeability and fluid flow. *PLoS ONE*, 12(9):e0184511, Sept. 2017.

[61] J. S. Young, C. E. Lumsden, and A. L. Stalker. The significance of the tissue pressure of normal testicular and of neoplastic (Brown-Pearce carcinoma) tissue in the rabbit. *J Pathol Bacteriol*, 62(3):313–333, July 1950.

[62] J. Zhao, H. Salmon, and M. Sarntinoranont. Effect of heterogeneous vasculature on interstitial transport within a solid tumor. *Microvasc. Res.*, 73(3):224–236, May 2007.